Thermal Hall transport in extended Kitaev models

Tsuyoshi Okubo,[1] Joji Nasu,[2] Takahiro Misawa,[3,4] and Yukitoshi Motome[5]

[1] *Institute for Physics of Intelligence, University of Tokyo, Tokyo, 113-0033, Japan*
[2] *Department of Physics, Tohoku University, Sendai 980-8578, Japan*
[3] *Beijing Academy of Quantum Information Sciences, Haidian District, Beijing 100193, China*
[4] *Institute for Solid State Physics, University of Tokyo, 5-1-5 Kashiwanoha, Kashiwa, Chiba 277-8581, Japan*
[5] *Department of Applied Physics, University of Tokyo, Tokyo, 113-8656, Japan*

The thermal Hall conductivity—a thermal current analog of the Hall conductivity for electric current—is a useful detector for exotic quasiparticles, such as Majorana fermions, which emerge from quantum many-body effects. For example, the half-integer quantization of the thermal Hall conductivity at the zero temperature limit has been regarded as direct evidence of the Majorana fermions. However, it remains unclear how the thermal Hall conductivity behaves at finite temperatures, even in the celebrated Kitaev model on a honeycomb lattice, which is one of the fundamental models for realizing the Majorana fermions in quantum magnets, despite the crucial importance to interprete the experimental observations. Here, using a finite-temperature tensor network method benchmerked by a thermal pure quantum state technique, we investigate the nature of the thermal Hall conductivity in the Kitaev model with additional interactions under a magnetic field. We find that the thermal Hall conductivity divided by temperature significantly overshoots the value of the half-integer quantization exhibits a hump while decreasing temperature, which is consistent with the experimental results on a candidate material α-$RuCl_3$. We also find that the field-direction dependence of the thermal Hall conductivity is consistent with the sign of the Chern number associated with the Majorana fermions, indicating its topological origin. We demonstrate that the additional off-diagonal interactions, known as the Γ and Γ' terms, significantly affect the thermal Hall conductivity. In particular, we show that positive Γ and negative Γ' lead to a remarkable enhancement of the thermal Hall conductivity in the intermediate temperature region. From the comparison with the classical counterpart, we show that the effects of the Γ term go beyond the classical picture, indicating significant quantum fluctuation effects, while those of the Γ' term is well captured at the classical level. Our findings establish a comprehensive theoretical framework for understanding the thermal Hall transport in Kitaev materials such as α-$RuCl_3$ and provide key insights for detecting the Majorana fermions in quantum spin liquids. Our developed method also bridges the gap between the theoretical predictions and experimental observations of the thermal Hall conductivity, providing a theoretical foundation for understanding its behavior in a wide range of strongly correlated materials.

I. INTRODUCTION

[we may break down the following paragraph into a general introduction of fractionalization, quantum spin liquid, and Kitaev QSL; see for instance Kato-san's paper on spin Seebeck] Quantum spin liquids (QSLs) are enigmatic states of quantum spin systems, which do not exhibit any spontaneous symmetry breaking even at zero temperature. Since the QSLs are the source of exotic emergent particles, such as Majorana fermions and anyons, the search for QSLs has been one of the central issues of modern condensed matter physics. Among various types of QSLs, the Kitaev QSL [1], which appears as the ground state of the Kitaev model on a honeycomb lattice, has attracted significant interest since its low-energy excitations can be rigorously described by noninteracting Majorana fermions. However, it remains a challenge to detect the Majorana fermions in candidate materials for the Kitaev QSL, since the Majorana fermions are charge-neutral and do not show any characteristic behaviors in response to electric or magnetic fields.

The thermal Hall conductivity is a promising observable for detecting the emergent Majorana fermions as they carry heat [1]. In the Kitaev model, perturbatively-introduced magnetic fields make the Majorana fermion bands topologically nontrivial. Accordingly, a chiral edge current appears, which is protected by the band topology characterized with a nonzero Chern number ν. Because the chiral edge current is an energy current of Majorana fermions, the thermal Hall conductivity κ_{xy} divided by temperature T is quantized as

$$\frac{\kappa_{xy}}{T} = \frac{1}{2}\frac{\pi k_{\rm B}^2}{6\hbar}\nu, \tag{1}$$

in the zero temperature limit, where $k_{\rm B}$ and $\hbar$ denote the Boltamann and Dirac constants, respectively. Here, ν takes ± 1 depending on the direction of the magnetic field. This quantized value is half of that for electrons with the same band topology, and hence, it is called the half-integer quantization. Detecting this peculiar behavior offers direct evidence of the Majorana fermions.

Strikingly, such a half-integer quantization was reported in the thermal Hall experiment for a quasi-two-dimensional van der Waals magnet α-$RuCl_3$ under a magnetic field [2]. Although α-$RuCl_3$ shows magnetic zigzag order at zero magnetic field [3–5], inelastic neutron scattering measurements suggest that applying a

magnetic field drives the system into a QSL [6]. The half-integer quantization observed in this field regime suggests that topologically-nontrivial Majorana bands are realized in this material. Similar quantization was observed even when subjected to an in-plane magnetic field, in contrast to the conventional thermal Hall effect of electrons that requires an out-of-plane field [7, 8]. It was also shown that field angle dependence of the thermal Hall conductivity is consistent with that in the Kitaev model, suggesting that the Majorana fermion bands in the real material have the same topology predicted by the Kitaev model [9].

However, there remains controversy on interpreting the observed thermal Hall transport as evidence of the Kitaev QSL. For example, the observed thermal Hall conductivity exhibits an overshooting behavior while decreasing temperature before converging to the half-integer quantized value. The origin of this behavior remains unresolved, although contributions from phonons [10, 11] and visons [12] were proposed. In addition, real compounds, including α-$RuCl_3$, may contain additional interactions not included in the Kitaev model, such as the Heisenberg interaction [13, 14], and the symmetric off-diagonal Γ and Γ' interactions [15–17], whose effects remain elusive.

Furthermore, several subsequent experiments on α-$RuCl_3$ have reported the absence of half-integer quantization. For instance, instead of the quantization in the transverse component, quantum oscillations were observed in the longitudinal thermal conductivity [18]. Additionally, other origins of the thermal Hall response were discussed, e.g., topological magnons [19–21], paramagnon [22], and phonons [23]. To resolve the origin of the thermal Hall conductivity observed in experiments, it is crucial to obtain reliable results by performing unbiased analysis of the thermal Hall conductivity in the Kitaev model and its extensions.

The thermal Hall transport in the pure Kitaev model has been well-understood in the limit of zero temperature and weak magnetic fields as mentioned above [1]. For finite-temperature properties, while several numerical simulation methods have been developed, they are applicable only at zero magnetic field, where the thermal Hall response vanishes, because of a negative sign problem [24–29]. A quantum Monte Carlo simulation based on a Majorana fermion representation has been performed for an effective model derived by a perturbation expansion with respect to the magnetic field [30]. It showed a non-monotonic temperature dependence in the thermal Hall conductivity with a weak peak at high temperature, but the result cannot explain the overshooting behavior observed in experiments since the peak value is much smaller than the half-integer quantized value.

The effects of non-Kitaev interactions have also been investigated based on perturbative arguments. For instance, it was shown that the Γ' term introduces an additional contribution to the gap of Majorana fermion band [31]; the gap increases (decreases) with a negative (positive) Γ' interaction, which might affect the finite-temperature behavior of the thermal Hall conductivity. In contrast, the effect of the Γ interaction appears at a higher-order expansion [32], suggesting weaker influence on the thermal Hall transport than that of Γ'. The same analysis also showed quantum phase transitions, which may lead to nontrivial effects. [refer to PRL 122, 147203 (2019)?] Nonetheless, all these analyses are based on perturbation theory justified for small Γ and Γ' in the zero temperature limit. Recently, an unbiased calculation using a tensor network method was conducted for the thermal Hall conductivity in the Kitaev-Heisenberg model [33], but the definition of energy current remains incomplete, as detailed later. Thus, for a comprehensive understanding of the effects of the non-Kitaev interactions on the thermal Hall transport, it is necessary to explore a theoretical framework with proper definition of energy current, beyond perturbation theory.

In this paper, we investigate the thermal Hall transport in an extended Kitaev model, which includes the symmetric off-diagonal interactions, Γ and Γ', using a finite-temperature tensor network method benchmarked with a thermal pure quantum state method. For comparison, we also perform classical Monte Carlo simulations in the classical limit of the model. We properly define the energy current from the model Hamiltonian and calculate the edge current in the systems with open boundaries. This treatment does not assume a specific origin for the thermal Hall transport, and includes all contributions on an equal footing. We find that the calculated thermal Hall conductivity shows a clear overshooting behavior similar to the experimental observations, suggesting that the experimentally-observed thermal Hall conductivity can be qualitatively explained by the extended Kitaev model. Through comprehensive analyses of the effects of Γ and Γ', we demonstrate that depending on the sign and type of these interactions, the thermal Hall conductivity can vary in both magnitude and sign at finite temperatures. In particular, we find that the thermal Hall conductivity is significantly enhanced by positive Γ and negative Γ' in an intermediate temperature range.

The organization of this paper is as follows. In Sec. II, we introduce the extended Kitaev model and give a brief overview of previous studies on this model. In Sec. III, we explain the procedure for calculating the thermal Hall conductivity in the extended Kitaev model. We also introduce the numerical methods used in this study, i.e., the exponential tensor renormalization (XTRG) method, the canonical thermal pure quantum state (cTPQ) method, and classical Monte Carlo simulations. In Sec. IV A, we show the temperature dependence of the thermal Hall conductivity for the pure Kitaev model under a magnetic field along the [111] direction. We also show the field-direction dependence of the thermal Hall conductivity. In Sec. IV B, we show how the off-diagonal interactions Γ and Γ' affect the temperature dependence of the thermal Hall conductivity. In Sec. IV C, we analyze the thermal Hall conductivity in

the classical limit of the Kitaev model. Section V is devoted to a summary and discussion.

II. MODEL

To investigate the thermal Hall conductivity in the Kitaev spin systems, we consider an extended Kitaev model containing the symmetric off-diagonal Γ and Γ' interactions on the honeycomb lattice. The Hamiltonian is given by

$$\mathcal{H} = \sum_{\gamma=x,y,z} \sum_{\langle i,j\rangle_\gamma} \mathcal{H}_{ij}^{\gamma} - \sum_{i,\gamma} h^{\gamma} S_i^{\gamma}, \tag{2}$$

with

$$\begin{aligned}\mathcal{H}_{ij}^{\gamma} = &\Big[K S_i^{\gamma} S_j^{\gamma} + \Gamma \left(S_i^{\mu} S_j^{\nu} + S_i^{\nu} S_j^{\mu}\right) \\ &+ \Gamma' \left(S_i^{\mu} S_j^{\gamma} + S_i^{\nu} S_j^{\gamma} + S_i^{\gamma} S_j^{\mu} + S_i^{\gamma} S_j^{\nu}\right)\Big] \qquad (3) \\ = &\sum_{\alpha,\beta=x,y,z} J_{\alpha\beta}^{\gamma} S_i^{\alpha} S_j^{\beta}, \qquad (4)\end{aligned}$$

where $\langle i,j\rangle_\gamma$ denotes nearest-neighbor pairs on γ-bonds on the honeycomb lattice [see Fig. 1(a)], and S_i^{γ} represents the γ component of the spin-1/2 operator at site i; (μ,ν,γ) is a cyclic permutation of (x,y,z), for example, $(\mu,\nu,\gamma) = (y,z,x)$ for the x-bond. The second term in Eq. (2) represents the Zeeman coupling to an external magnetic field $\boldsymbol{h} = (h^x, h^y, h^z)$.

A microscopic origin of the Kitaev interaction K in Eq. (2) was proposed for effective $j_{\rm eff} = 1/2$ moments in spin-orbit coupled Mott insulating systems [34]. It was pointed out that magnetic ions with t_{2g}^5 electron configurations comprise the spin-orbit entangled $j_{\rm eff} = 1/2$ states under the strong spin-orbit coupling, and exchange processes with indirect hoppings via ligands generate the bond-dependent Kitaev-type interactions between the $j_{\rm eff} = 1/2$ moments in edge-sharing octahedral coordinates. The symmetric off-diagonal interactions Γ and Γ' were introduced as additional contributions arising from different exchange processes [15]. On one hand, the Γ interaction is derived by the exchange process including both direct and indirect hoppings, which can be relevant in Kitaev candidate materials [17, 35, 36]. On the other hand, the Γ' interaction is induced by symmetry lowering of the octahedra surrounding magnetic ions from the cubic symmetry, inevitably existing in real materials [15]. The realistic values of interaction parameters have been extensively discussed for the Kitaev candidate materials [37–40]. Most theoretical works have suggested $K < 0$ and $\Gamma > 0$ for the primary candidate α-$RuCl_3$, although the sign of Γ' remains under debate.

The K-Γ model, which is given by Eq. (2) with $\Gamma' = 0$, has been intensively studied as a simplified realistic model, by using various theoretical methods, such as the exact diagonalization [41, 42], the density matrix renormalization group method [43], the infinite projected entangled pair state method [44, 45], a variational approach [46], the spin-wave theory [47], and a classical spin approach [48]. In the classical limit, this model exhibit macroscopic degeneracy. Quantum fluctuations lift this degeneracy, but the detailed phase diagram remains controversial. The introduction of the Γ' interaction to the K-Γ model with $K < 0$ and $\Gamma > 0$ induces magnetically ordered phases: a positive Γ' stabilizes a ferromagnetic phase and a chiral spin ordered phase with nonzero spin scalar chirality [49, 50], and a negative Γ' induces the zigzag order, which has been observed in Kitaev candidate materials at low temperatures [44, 51–53]. Thus, the K-Γ-Γ' model in Eq. (2) might be suitable for investigating the relevant effects of symmetric off-diagonal interactions on the thermal Hall conductivity in real compounds including α-$RuCl_3$.

In the following sections, we consider the ferromagnetic Kitaev interaction by setting $K = -1$, which naturally arises from the exchange process in the t_{2g}^5 systems [34]. For Γ and Γ', we consider both positive and negative cases. We take $k_{\rm B} = \hbar = 1$ and set the length of the primitive translation vector of the honeycomb lattice to

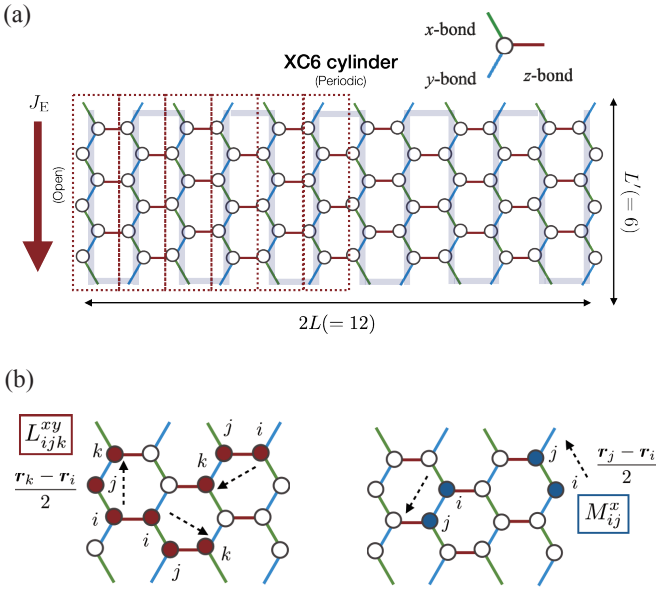

FIG. 1. (a) Schematic view of the honeycomb lattice structure with $(L, L') = (6, 6)$, consisting of 72 sites, which is typically used in the XTRG calculations. The inset represents γ-bonds in the Hamiltonian in Eq. (2). We impose the periodic and open boundary conditions along the vertical and horizontal directions, respectively. We consider the thermal current $J_{\rm E}$ in a downward direction indicated by the arrow. In the tensor network simulation, we consider a snake-like matrix product operators indicated by the gray thick line behind the lattice. (b) Graphical representations of the three-body ($L_{ijk}^{\gamma\gamma'}$) and the two-body (M_{ij}^{γ}) terms in the definition of the thermal current in Eq. (6). [omit "XC6 cylinder" in (a)?] [indicate "$l = 1$", "$l = 2$", ... above or below the dotted boxes in (a)?] [place the boxes in (b) above each panel?]

the unit length. We typically compute physical quantities for the model on a finite-size cluster with $(L, L') = (6, 6)$ shown in Fig. 1(a), including $N_s = 2 \times L \times L' = 72$ spins.

III. METHOD

In this section, we introduce the methods used in this study. First, we define the energy current and the thermal Hall conductivity in Sec. III A. Then, we describe two numerical methods for calculating the finite-temperature behaviors: a tensor network method called the XTRG method in Sec. III B and the cTPQ method in Sec. III C. We employ the former for main calculations on the $(L, L') = (6, 6)$ cluster introduced above, and use the latter for the benchmark in smaller size clusters. Finally, in Sec. III D, we briefly describe the method of classical Monte Carlo simulation to study a classical counterpart to the model.

A. Thermal Hall conductivity

To investigate the thermal Hall conductivity in Kitaev systems, we define the energy polarization as [30, 54]

$$\boldsymbol{P}_{\mathrm{E}} = \sum_{\alpha,\beta,\gamma} \sum_{\langle i,j\rangle_\gamma} \frac{\boldsymbol{r}_i + \boldsymbol{r}_j}{2} J^\gamma_{\alpha\beta} S^\alpha_i S^\beta_j - \sum_{i,\gamma} \boldsymbol{r}_i h^\gamma S^\gamma_i, \quad (5)$$

where $\boldsymbol{r}_i$ is the position of site i. From the commutation relation between the Hamiltonian and $\boldsymbol{P}_{\mathrm{E}}$, the energy current $\boldsymbol{J}_{\mathrm{E}}$ is obtained as

$$\begin{aligned}\boldsymbol{J}_{\mathrm{E}} &= i\,[\mathcal{H}, \boldsymbol{P}_{\mathrm{E}}] \\ &= \sum_{\gamma,\gamma'} \sum_{\langle i,j,k\rangle_{\gamma,\gamma'}} \frac{\boldsymbol{r}_k - \boldsymbol{r}_i}{2} L^{\gamma\gamma'}_{ijk} + \sum_{\gamma} \sum_{\langle i,j\rangle_\gamma} \frac{\boldsymbol{r}_j - \boldsymbol{r}_i}{2} M^\gamma_{ij},\end{aligned} \quad (6)$$

where $\langle i, j, k\rangle_{\gamma,\gamma'}$ represents three neighboring sites consisting of two nearest-neighbor pairs $\langle i, j\rangle_\gamma$ and $\langle j, k\rangle_{\gamma'}$ connected at site j. The operator $L^{\gamma\gamma'}_{ijk}$ is the contribution from three-spin correlations,

$$L^{\gamma\gamma'}_{ijk} = \sum_{\alpha,\beta,\alpha',\beta',\gamma''} J^\gamma_{\alpha\beta} J^{\gamma'}_{\alpha'\beta'} \epsilon_{\alpha\gamma''\alpha'} S^\beta_i S^{\gamma''}_j S^{\beta'}_k, \quad (7)$$

and M^γ_{ij} represents the contribution from two-spin correlations,

$$M^\gamma_{ij} = \sum_{\alpha,\beta,\gamma',\gamma''} J^\gamma_{\alpha\beta} h_{\gamma'} \epsilon_{\gamma'\alpha\gamma''} \left(S^{\gamma''}_i S^\beta_j - S^\beta_i S^{\gamma''}_j \right), \quad (8)$$

where $\epsilon_{\alpha\beta\gamma}$ denotes the completely antisymmetric tensor, which comes from the commutation relation between spins. The schematic pictures of these operators are shown in Fig. 1(b). It is worth noting that the three-spin product in $L^{\gamma\gamma'}_{ijk}$ coincides with the effective magnetic field derived by third-order perturbations with respect to $\boldsymbol{h}$ in the Majorana representation of the Kitaev model [1, 30]. The effective magnetic field induces the next nearest-neighbor hoppings, which open an excitation gap in the noninteracting Majorana fermion bands and result in nontrivial band topology with nonzero Chern numbers [1]. Thus, the $L^{\gamma\gamma'}_{ijk}$ term in Eq. (6) is expected to induce a chiral edge current contributing to the thermal Hall effect, at least in the pure Kitaev model with weak magnetic fields. In contrast, the M^γ_{ij} term is proportional to the magnetic field, which is not present in the perturbation. These two contributions will be examined separately in Sec. IV.

We note that our definition of the energy current is different from that used in Ref. [33], where the energy current is defined through the commutation relation of the local Hamiltonians. The energy current should be defined through the commutation relation of the total Hamiltonian and the total energy polarization as given in Eq. (6). The energy current used in Ref. [33] neglects the position dependence included in the definition of $\boldsymbol{P}_{\mathrm{E}}$. This could explain why κ_{xy} in Ref. [33] is significantly smaller than the value obtained in this study.

In the following calculations, we compute the thermal Hall current as the summation of the energy current along the zigzag chains on the honeycomb lattice. The energy current on each zigzag chain, $J^{\parallel}_{\mathrm{E},l}$ labeled by l, includes the contributions from local currents on the segments inside a box surrounding the chain and across its right edge, which are shown in Fig. 1(a). We compute $J^{\parallel}_{\mathrm{E}}$ by regarding each term in Eq. (6) as the current density at $(\boldsymbol{r}_i + \boldsymbol{r}_j)/2$. Then, we obtain the contribution to the thermal Hall current by summing up $J^{\parallel}_{\mathrm{E}}$ over half of the system from the left edge to the center of the system, which is defined as

$$J^{\parallel}_{\mathrm{E}} = \sum_{l=1}^{L} J^{\parallel}_{\mathrm{E},l}. \quad (9)$$

Note that the summation over the whole system cancels out at any temperature due to the symmetry. By taking the derivative of $J^{\parallel}_{\mathrm{E}}$ with respect to temperature, we obtain the thermal Hall conductivity as

$$\kappa_{xy} = \frac{2}{L'} \frac{d\langle J^{\parallel}_{\mathrm{E}}\rangle_T}{dT}, \quad (10)$$

where $\langle\cdots\rangle_T$ represents the thermal average at temperature T. [need to mention about the factor of $2/L'$?]

B. Tensor network method

Let us first introduce the tensor network method employed in our study. To calculate finite-temperature properties of the model given by Hamiltonian $\mathcal{H}$, we approximate the density matrix of the system at an inverse temperature β, $\rho(\beta) = e^{-\beta\mathcal{H}}$, by a matrix product operator (MPO) with bond dimension D [see Fig. 2(a)]. In the actual calculations, the string of the MPO is arranged in

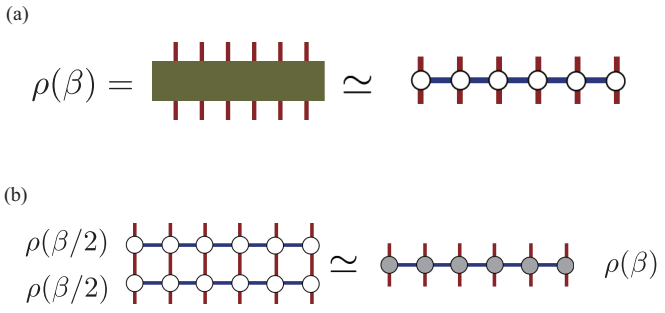

FIG. 2. Tensor network diagram for the density operator approximation. (a) The density matrix is approximated as a MPO with bond dimension D. The horizontal line in the right panel corresponds to the gray line in Fig. 1(a). (b) The density matrix at β is calculated as $\rho(\beta) = \rho(\beta/2)\rho(\beta/2)$. The bond dimension of the obtained $\rho(\beta)$ is truncated at D through the standard optimization procedure of MPS.

a snake form on the honeycomb cluster, as indicated by the gray line in Fig. 1(a).

To optimize the tensors in an MPO as the density matrix at β, we employ the XTRG approach [55], which has been successfully used to calculate finite temperature properties of extended Kitaev models [56, 57]. In the XTRG method, we calculate the density matrix at β through the relationship

$$\rho(\beta) = \rho(\beta/2)\rho(\beta/2). \tag{11}$$

When $\rho(\beta/2)$ is represented by an MPO with the bond dimension D, $\rho(\beta)$ becomes an MPO with the bond dimension D^2. We approximate $\rho(\beta)$ by an MPO with bond dimension D through the standard optimization procedure for the matrix product states (MPS) [55] [see Fig. 2(b)]. In the optimization, we employ the two-site update, resulting in the total computational cost scales as $O(D^4)$. As the initial condition of the XTRG method, we prepare $\rho(\beta_0)$ with $\beta_0 = 10^{-7}$ through the approximated form $\rho(\beta_0) \simeq 1-\beta_0\mathcal{H}$, where the Hamiltonian is represented as an MPO. We calculate the expectation value of an operator O through thus obtained $\rho(\beta)$ as $\langle O\rangle = \mathrm{Tr}[O\rho]/\mathrm{Tr}\rho$ (note that the density matrix is not normalized). The temperature derivative of $\langle O\rangle$ is computed by numerical differentiation. In the following, we mainly show the data with $D = 500$ for the $(L, L') = (6, 6)$ cluster. Several benchmark calculations for different values of D and different cluster shapes are shown in Appendix A.

C. Thermal pure quantum state

Next, we describe the cTPQ state method [58], which enables us to calculate finite-temperature properties of quantum many-body systems using the power method. We note that several similar methods were independently proposed [59–62] before the proposal of the cTPQ state method [58]. The cTPQ state is constructed as

$$|\Phi^p_{\mathrm{cTPQ}}(\beta)\rangle = \exp\Big[-\frac{\beta}{2}\mathcal{H}\Big]|\Phi^p_{\mathrm{rand}}\rangle, \tag{12}$$

where $|\Phi^p_{\mathrm{rand}}\rangle$ is the pth initial random vector, which is uniformly distributed on the N_{H}-dimensional hypersphere (N_{H} is the dimension of the Hilbert space of the given system). Any local physical quantity at inverse temperature β can be calculated as the expectation values of $|\Phi^p_{\mathrm{cTPQ}}(\beta)\rangle$, i.e.,

$$\langle A(\beta)\rangle = \frac{\langle\Phi^p_{\mathrm{cTPQ}}(\beta)|A|\Phi^p_{\mathrm{cTPQ}}(\beta)\rangle}{\langle\Phi^p_{\mathrm{cTPQ}}(\beta)|\Phi^p_{\mathrm{cTPQ}}(\beta)\rangle}. \tag{13}$$

We numerically obtain the cTPQ state by

$$\exp\Big[-\frac{\beta}{2}\mathcal{H}\Big]|\Phi^p_{\mathrm{rand}}\rangle = U(\Delta\tau)^k|\Phi^p_{\mathrm{rand}}\rangle, \tag{14}$$

where $\beta = k\Delta\tau$ and

$$U(\Delta\tau) = \exp\Big[-\frac{\Delta\tau}{2}\mathcal{H}\Big] \sim \sum_{n=0}^{n_{\max}} \frac{1}{n!}\left(-\frac{\Delta\tau}{2}\mathcal{H}\right)^n. \tag{15}$$

In the following calculations, we take $n_{\max} = 6$ and $\Delta\tau = 0.02$, for which we confirm good convergence of physical quantities in the calculated temperature region. In actual calculations, we use $\mathcal{H}\Phi$ [63–65], where the cTPQ state method is implemented.

The cTPQ state method provides the numerically exact results within the statistical errors, which are defined by the statistical distribution of the initial random vectors. To estimate the statistical errors of the cTPQ method, we employ the bootstrap method [64]. Benchmark results of the cTPQ state method in the pure Kitaev model are shown in Appendix B. We also compare the results of the cTPQ state method with those of the XTRG method in Appendix C.

D. Classical Monte Carlo simulation

Finally, we describe the method of classical Monte Carlo simulations. In this method, an $S = 1/2$ spin at each site is regarded as a classical vector with length 1/2. The classical spin at site i is parameterized by θ_i and ϕ_i as $\boldsymbol{S}_i = \frac{1}{2}(\sin\theta_i\cos\phi_i, \sin\theta_i\sin\phi_i, \cos\theta_i)$. In the calculations of the thermal average, the integral $\int\prod_i d\phi_i d\theta_i \sin\theta_i$ is evaluated using the Markov-chain Monte Carlo method. To accelerate computations and avoid trapping spin configurations in local minima, we use the replica exchange method [66]. In the simulations, we prepare 48 replicas with different temperatures. We perform 10 000 000 MC steps for measurements after 10 000 MC steps for thermalization in the 800-site cluster with $(L, L') = (10, 40)$. The temperature derivative of $\langle O\rangle$ is evaluated by the correlation with $\mathcal{H}$ as

$$\frac{d\langle O\rangle}{dT} = \frac{\langle O\mathcal{H}\rangle - \langle O\rangle\langle\mathcal{H}\rangle}{T^2}, \tag{16}$$

which gives accurate estimates compared to numerical differentiation.

IV. RESULT

In this section, ...

A. Pure Kitaev model

1. *Magnetic field along [111] direction*

We begin with the ferromagnetic Kitaev model ($K = -1$ and $\Gamma = \Gamma' = 0$) in an applied magnetic field along the [111] direction ($h^x = h^y = h^z$). In this setup, we expect κ_{xy}/T to be quantized at a positive value of $\pi/12$ for small magnetic fields $h = |\boldsymbol{h}|$ in the zero temperature limit [1]. Figures 3(a)-3(c) show the temperature dependence of the specific heat C, the magnetic moment along the magnetic field $M_{\parallel}$, and the flux density W, respectively given by

$$C = \frac{\langle \mathcal{H}^2 \rangle - \langle \mathcal{H} \rangle^2}{T^2}, \tag{17}$$

$$M_{\parallel} = \langle \boldsymbol{M} \rangle \cdot \frac{\boldsymbol{h}}{|\boldsymbol{h}|}, \quad \boldsymbol{M} = \frac{1}{N_{\rm s}} \sum_i \boldsymbol{S}_i, \tag{18}$$

$$W = \frac{1}{N_{\rm h}} \sum_p \langle W_p \rangle, \quad W_p = 2^6 \prod_{i \in p} S_i^{\gamma_i}, \tag{19}$$

where p runs over all hexagons in the honeycomb lattice and $N_{\rm h}$ is the number of hexagons; γ_i denotes the bond component that does not belong to the edges of p at site i.

We first discuss the temperature dependence of the specific heat C. As shown in Fig. 3(a), we observe clear double-peak structures at each magnetic field, which appear to evolve smoothly from the characteristic feature of the Kitaev model at zero field arising from fractionalization of spins into Majorana fermions [24, 25]. By increasing the magnetic field, the low-temperature peaks shift to higher temperatures, while the high-temperature peaks are almost independent of the magnetic field. This behavior of the low-temperature peak is not observed in the calculations where the magnetic field is introduced perturbatively [30], suggesting the importance of nonperturbative effects.

In the low-field region for $h \lesssim 0.03$, the specific heat exhibits non-smooth temperature dependence at low temperatures. The origin of this behavior might be the finite bond dimension D in the XTRG calculations. Nevertheless, the magnetic-field dependence of the low-temperature peak appears to be consistent with the previous studies [29, 57, 67], where the peak moves toward a lower temperature under a weak magnetic field, while it shifts toward a higher temperature as the magnetic field is increased to $h \gtrsim 0.02$. The Kitaev model is known to exhibit a quantum phase transition from a topological chiral spin liquid to a polarized state at $h_c \simeq 0.02$ [68]. The above behavior may be associated with a signature of this transition. In contrast, in the higher-field region for $h \gtrsim 0.04$, the specific heat exhibits smooth temperature dependence down to $T = 0.01$. Therefore, it is plausible that $D = 500$ is sufficient to capture the thermal properties of the Kitaev model in this field region. Further discussions on the D dependence are shown in Appendix A.

Next, we discuss the temperature dependence of the magnetization $M_{\parallel}$ and the flux density W shown in Figs. 3(b) and 3(c), respectively. As expected, by increasing the magnetic field, $M_{\parallel}$ monotonically increases, reaching more than 60% of the saturation value of 0.5 for $h \gtrsim 0.05$ at low temperatures. Since an applied magnetic field inducing nonzero magnetization renders the flux operator on each hexagonal plaquette a nonconserved quantity, W monotonically decreases by increasing the magnetic field, down to ~ 0.4 for $h \gtrsim 0.05$ at low temperatures, which is significantly lower than $W = 1$ expected for the ideal Kitaev QSL. We note that both $M_{\parallel}$ and W decrease rapidly around at $h_c \simeq 0.02$.

Figure 3(d) displays the temperature dependence of the thermal Hall conductivity divided by temperature, κ_{xy}/T. As this is obtained by the temperature derivative of the energy current through Eq. (10) with Eq. (9), let us discuss the behavior of the energy current first. Figure 4 shows the temperature dependence of the total energy current $\langle J_{\rm E}^{\parallel} \rangle_T$ defined in Eq. (9) at two representative magnetic fields, $h = 0.04$ and $h = 0.08$. We find that $\langle J_{\rm E}^{\parallel} \rangle_T$ monotonically decreases while decreasing temperature, starting from $\langle J_{\rm E}^{\parallel} \rangle_T = 0$ in the high-temperature limit. This behavior indicates that κ_{xy} is positive in the entire temperature range, which is consistent with the expectation in the zero temperature limit. In addition, $\langle J_{\rm E}^{\parallel} \rangle_T$ exhibits an inflection point at an intermediate temperature, indicating that κ_{xy} has a peak at the corresponding temperatures, as discussed below. Notably, the temperature of the inflection point appears to correlate with the peak temperature of the specific heat in Fig. 3(a).

Figure 4 also plots the contributions from each zigzag chain, $\langle J_{{\rm E},l}^{\parallel} \rangle_T$. We find that the amplitude of the energy current is largest at the edge ($l = 1$), and rapidly decreases toward the center of the system ($l = 6$) [see Fig. 1(a)]. This result demonstrates that the energy current is dominated by the edge current, similar to the chiral edge current originating from the topologically-nontrivial Majorana band structure predicted by the perturbation theory. Note that the contributions from the center region are sufficiently small, indicating that the employed system size, $L = 6$, is large enough to capture the essential features of this edge current. Interestingly, we observe the edge current even for high fields well beyond $h_c \simeq 0.02$. We also find that the current amplitude decays more rapidly toward the center as the magnetic

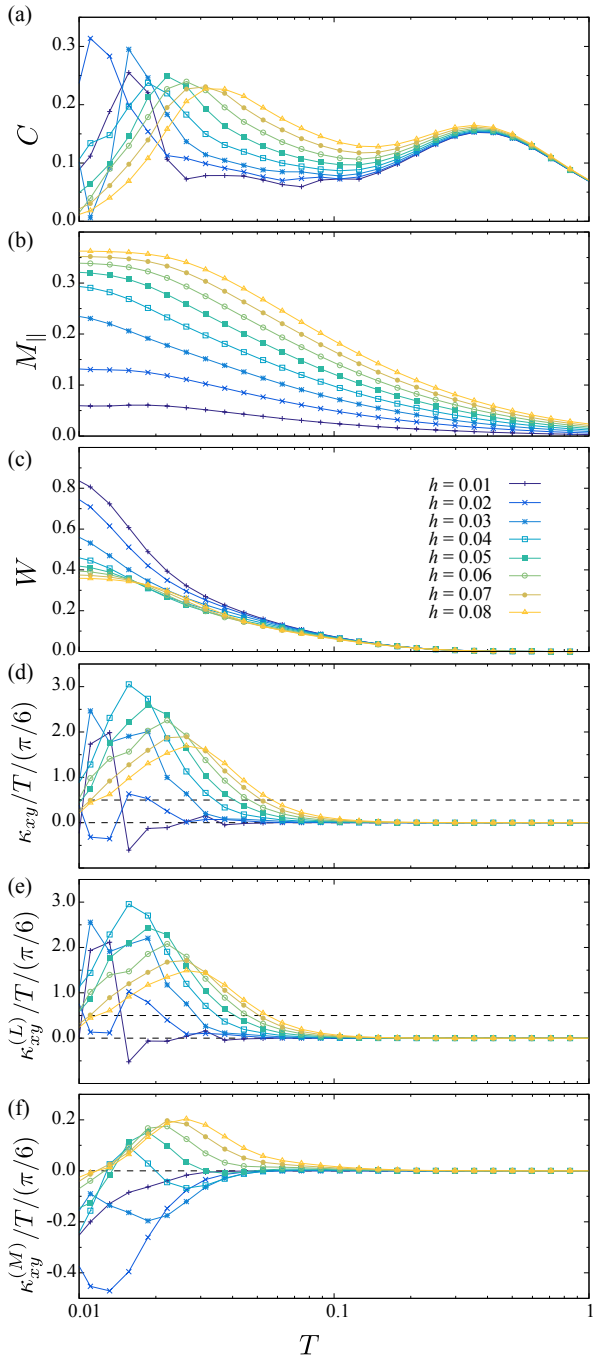

FIG. 3. Temperature dependence of (a) the specific heat [Eq. (17)], (b) the magnetic moment [Eq. (18)], (c) the flux density [Eq. (19)], and (d) the thermal Hall conductivity κ_{xy} [Eq. (10)] divided by T of the ferromagnetic Kitaev model for several values of the external magnetic field parallel to the [111] direction ($h = |\boldsymbol{h}|$). (e), (f) Contributions from the three-spin term in Eq. (7) and the two-spin term in Eq. (8) to κ_{xy}/T, respectively. The data in (d), (e), and (f) are plotted in units of $\pi/6$, and two horizontal dashed lines in each figure indicate $\kappa_{xy}/T = 0$ and the half-integer quantized value $\pi/12$.

field increases. This behavior might be explained by the increase in the excitation gap of quasiparticles carrying energy.

Then, let us discuss the temperature dependence of κ_{xy}/T shown in Fig. 3(d). First of all, κ_{xy}/T is overall positive, except for small h and low T, and exhibits a nonmonotonic temperature dependence with a clear peak structure, which shifts to higher temperatures with increasing h. These behaviors are expected from $\langle J_{\mathrm{E}}^{\parallel}\rangle_T$ in Fig. 4. Surprisingly, the peak of κ_{xy}/T largely exceeds the half-integer quantized value indicated by the broken line in Fig. 3(d). It appears to develop with increasing h up to $h \simeq 0.04$ and slowly decline for higher h. Such an overshooting behavior was not observed in the previous numerical calculations which treated the magnetic fields as the effective three-spin interactions [30], or defined the energy current in a simplified way [33]. Our results indicate that full quantum calculations with proper definition of the energy current can explain the overshooting behavior observed in experiments by purely magnetic origin, without considering contributions from phonons [10, 11]. [should we comment on the relation to Joy2022?]

We note that while κ_{xy}/T takes a value around the half-integer quantization $\pi/12$ at the lowest temperature calculated, it does not exhibits any clear signature of the convergence to the quantization, even when the magnetic field is sufficiently small. This is presumably due to the finite bond dimension D, finite-size effects, and insufficiently low temperatures. First, as discussed for the specific heat above, the bond dimension $D = 500$ is not sufficient to obtain reliable results at low temperatures for $h \lesssim 0.04$. Second, for the finite-size effects, the excitation gap is expected to be smaller for smaller h, leading to a larger spatial extension of the edge current into the bulk. This causes an overlap between the contributions from both edges in the finite-size cluster, thereby hampering accurate estimates of the edge current. Lastly, asymptotic quantization is expected to occur for sufficiently lower temperatures compared to the excitation gap of topological quasiparticles, whose precise value is not known beyond the perturbation theory. Sophisticated methods are required to further study this issue.

To gain more insights into the thermal Hall conductivity, we separate it into the two parts $\kappa_{xy}^{(L)}$ and $\kappa_{xy}^{(M)}$, which are contributions from the three-spin and two-spin correlations defined in Eqs. (7) and (8), respectively. Figures 3(e) and 3(f) show the temperature dependence of $\kappa_{xy}^{(L)}$ and $\kappa_{xy}^{(M)}$, respectively. We find that the three-spin part $\kappa_{xy}^{(L)}/T$ dominantly contributes to the total κ_{xy}/T across all magnetic fields. In contrast, the contribution from two-spin part $\kappa_{xy}^{(M)}/T$ is an order of magnitude smaller than that from the three-spin part and plays a minor role.

From these observations, we discuss the origin of the thermal Hall effect. Since the three-spin terms in Eq. (7) is represented by the effective magnetic field obtained from the third-order perturbations for $\boldsymbol{h}$ in the Majo-

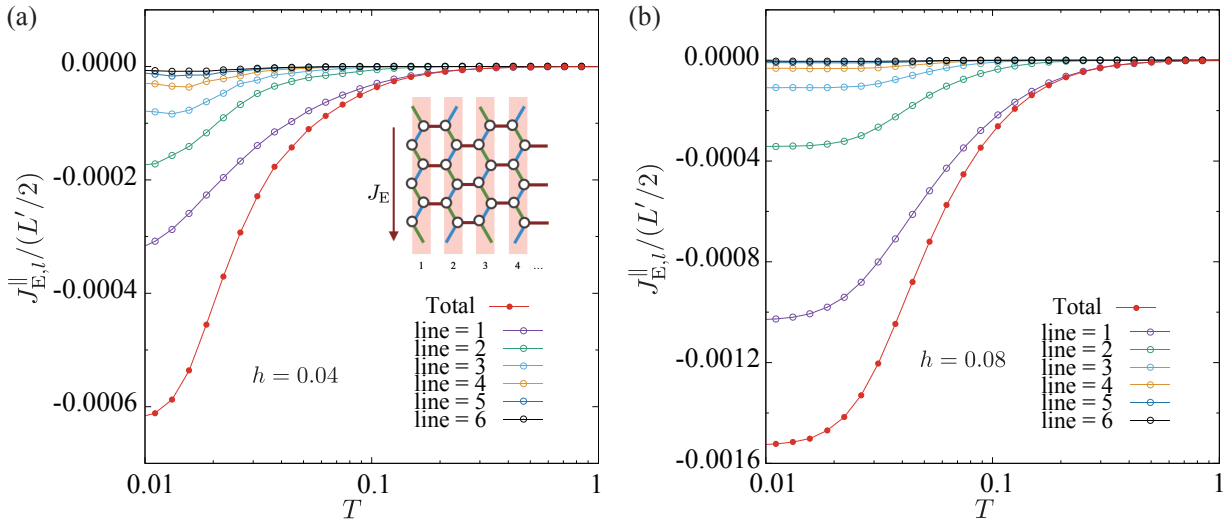

FIG. 4. Temperature dependence of the energy current of the ferromagnetic Kitaev model at (a) $h = 0.04$ and (b) $h = 0.08$. In addition to the total energy current, the contribution from each line is shown; see Eq. (9). [need "$\langle\cdots\rangle_T$" in the labels on the vertical axes? also need the label "$\langle J^{\parallel}_{\mathrm{E}}\rangle_T/(L'/2)$"?]

rana fermion representation, $\kappa_{xy}^{(L)}$ is expected to include the contributions predominantly from the topological gap opening in the emergent Majorana fermion system. In contrast, the two-spin terms in Eq. (8) scale linearly with the magnetic field, suggesting that $\kappa_{xy}^{(M)}$ includes effects beyond the Majorana fermion picture, which may be better described by magnon excitations. Since κ_{xy} is dominated by $\kappa_{xy}^{(L)}$ as discussed above, its behavior in the calculated field range is consistently understood by the topological Majorana fermion picture rather than the magnon picture. Note that the magnon contributions should monotonically decrease with increasing the magnetic field [69]. Our results suggest that Majorana-like excitations play a dominant role in the thermal Hall effect exhibiting a large peak at an intermediate temperature, in a wide range of the magnetic field even beyond $h_c \simeq 0.02$.

2. *Field-direction dependence*

In this section, we examine the field-direction dependence of physical quantities in the pure Kitaev model. Here we consider three cases by taking the magnetic field direction parallel to [111], [11$\bar{2}$], and [$\bar{1}$10]. Note that the data for [111] are common to those in the previous section. When we take the (S^x, S^y, S^z) axes to the cartesian coordinates connecting the magnetic ion and the surrounding ligands in the edge-sharing honeycomb network of octahedra [34], the [111] direction is out-of-plane, while [11$\bar{2}$] and [$\bar{1}$10] are in-plane. [better to show the figure?] The perturbation theory for the magnetic field predicts changes in the band topology in the Majorana fermion bands: the gap in the Majorana excitations opens in proportion to the product of three field components $h^x h^y h^z$, and the Chern number ν changes its sign depending on the sign of $h^x h^y h^z$ [1]. This suggests that κ_{xy}/T in Eq. (1) changes its sign depending on the sign of $h^x h^y h^z$. For instance, κ_{xy}/T is expected to be positive and negative for the [111] and [11$\bar{2}$] fields, respectively, whereas it vanishes for [$\bar{1}$10]. We examine such behaviors by numerics beyond the perturbation theory.

Figure 5 shows the results for $h = 0.04$ and $h = 0.08$. We find that the specific heat and the magnetization do not show significant changes across different field directions as shown in Figs. 5(a) and 5(b), whereas the flux density significantly decreases for the [$\bar{1}$10] direction as shown in Fig. 5(c). This behavior might be related to the presence of low-energy excitations, as the gap does not open in the Majorana excitations for the field in this direction in the perturbation theory [1].

The thermal Hall conductivity exhibits strong field-direction dependence, as expected in the perturbation theory. As shown in Fig. 5(d), we find that κ_{xy}/T reverses its sign from positive to negative by changing the field direction from [111] to [11$\bar{2}$]. We also find that the three-spin contribution $\kappa_{xy}^{(L)}$ is dominant and governs the sign change of the total κ_{xy} in both cases. In addition, κ_{xy}/T is vanishingly small for [$\bar{1}$11]. These results suggest that the topological Majorana fermion picture provides a plausible explanation for the field-direction dependence of the thermal Hall effect in the wide range of the field intensity beyond the perturbative region.

We note that the vanishment of κ_{xy}/T for the [$\bar{1}$10] field for all temperatures can be understand from the symmetry of the Hamiltonian. The Hamiltonian in Eq. (2) is invariant under the following two simultaneous operations: the C_2 rotation along the [$\bar{1}$10] axis in spin

space transforming (S^x, S^y, S^z) to $(-S^y, -S^x, -S^z)$ and the rotation of the honeycomb plane along the z bond in real space exchanging the x and y bonds. The rotation of the honeycomb plane inverts the component of the position vector $\boldsymbol{r}$ along the zigzag edge, and thereby, the thermal current along the zigzag edge should be zero. Note that this symmetry argument is applicable in the presence of the Γ and Γ' interactions.

It is worth noting that the sign change in κ_{xy}/T was also predicted by the topological magnon picture [69–71]. In this picture, however, the sign is opposite to that of the topological Majorana fermion picture.

B. Effect of non-Kitaev interactions

In this subsection, we investigate the effects of the symmetric off-diagonal interactions, the Γ and Γ' terms, on the thermal Hall conductivity. Based on the magnetic field dependence in the Kitaev model, the elementary excitations appear to be dominated by Majorana fermions rather than magnons, particularly in the weak magnetic field limit. As we mentioned in Introduction, according to the perturbative theory in the Majorana fermion representation, it is shown that the negative Γ' enhances the Majorana gap [72]. Therefore, the thermal Hall conductivity is expected to be enhanced by the negative Γ'. In contrast to Γ', the perturbative expansion with respect to Γ is not straightforward, and it remains unclear how Γ affects the thermal Hall conductivity. Here, we examine the impact of the Γ' and Γ terms in the original spin representation without assuming the Majorana excitations.

1. *Symmetric off-diagonal interaction* Γ'

First, we consider the effect of the Γ' interaction on κ_{xy}/T under two representative magnetic fields along the [111] direction, $h = 0.04$ and $h = 0.08$. In Figs. 6(a)–6(c), we show several physical quantities for $-0.02 \leq \Gamma' \leq 0.02$. Here, we set $\Gamma = 0$ to only examine the effects of Γ' term. We find that Γ' does not significantly change the overall temperature dependence of the specific heat, although low-temperature peaks shift slightly to higher (lower) temperatures for negative (positive) Γ'. We also find that the magnetization increases (decreases) monotonically for the negative (positive) Γ'. In perturbation theory for the Γ' term [72], it is shown that the gap is proportional to $-\Gamma'/|K|$. This result indicates that the effective magnetic field increases (decreases) for the negative (positive) Γ'. Therefore, the observed Γ' dependence of the magnetization is consistent with perturbation theory. In contrast to the magnetization, the flux does not show considerable changes as a function of Γ'.

Figs. 6(d)–6(f) show the temperature dependence of κ_{xy}/T for the same values of Γ'. Although the effects on the bulk physical quantities are small as we have shown above, Γ' significantly changes κ_{xy}/T; when we decrease Γ' from 0.02, the peak of κ_{xy}/T shifts to higher temperature while its height increases. In particular, for the negative (positive) Γ', an increase of its absolute value results in an enhancement (suppression) of κ_{xy}/T. Such sign-dependent changes in κ_{xy} are broadly consistent with the results from perturbation theory [31].

We also find that Γ' monotonically reduces both the three-body part and the two-body part of κ_{xy}; With increasing from $\Gamma' = -0.02$, $\kappa_{xy}^{(L)}$ is suppressed and its peak shifts toward lower temperatures [Fig. 6(e)], similar to the total thermal Hall conductivity [Fig. 6(d)]. On the other hand, $\kappa_{xy}^{(M)}$ exhibits a sign change from positive to negative [Fig. 6(f)]. For $\Gamma' \geq 0.01$, there is a competition between the positive $\kappa_{xy}^{(L)}$ and the negative $\kappa_{xy}^{(M)}$. As a result, at $\Gamma' = 0.02$ and $h = 0.04$, the total κ_{xy}/T turns negative around $T = 0.04$, although its absolute value is small.

2. *Symmetric off-diagonal interaction* Γ

Next, we investigate the effects of the Γ term on κ_{xy}/T under a magnetic field parallel to the [111] direction. Again, we consider two representative magnetic fields, $h = 0.04$ and $h = 0.08$. In Figs. 8(a)–8(c), we show the temperature dependence of the specific heat, the magnetization, and the flux for $-0.02 \leq \Gamma \leq 0.02$. Although the magnitudes of Γ are relatively small, we find that the low-temperature peaks of the specific heat show significant change. For negative Γ, the peak shifts to a higher temperature, with an increase in its height. Similarly, the magnetization increases for negative Γ. For positive Γ, we observe the opposite effects. We can also see sign-dependent changes in the flux around the intermediate temperature region $T \sim 0.03$, although the effect is not so significant.

As shown in Figs. 8(d)–8(f), we find that the Γ term has a significant impact on the thermal Hall conductivity. Negative Γ suppresses κ_{xy}/T for both $h = 0.04$ and $h = 0.08$. For positive Γ, we observe different behaviors between $h = 0.04$ and $h = 0.08$. For $h = 0.04$, positive Γ strongly suppresses κ_{xy}/T, and it becomes even negative for $\Gamma = 0.02$. In contrast to $h = 0.04$, we observe that positive Γ enhances κ_{xy}/T. Such large changes in κ_{xy}/T by small Γ seem to be different from the result of perturbation theory, where contributions from Γ appear only at third order [32].

This magnetic field-dependent behavior might be related to the large magnitude of $\kappa_{xy}^{(M)}/T$ observed for positive Γ. For $\Gamma \leq 0$, $\kappa_{xy}^{(L)}$ dominates the total κ_{xy}/T. However, for $\Gamma = 0.01$ and 0.02 at $h = 0.04$, the low-temperature value of $\kappa_{xy}^{(M)}/T$ significantly changes as shown in Fig. 8(f).This abrupt change may indicate the presence of a phase transition from the Kitaev QSL to another phase, such as a spin nematic state, as suggested by infinite tensor network calculations at zero temperature [44].

C. Classical limit

In this section, we show the results obtained by applying the classical approximation to Eq. (2) to compare them with those of the quantum spin model shown above. First, we focus on the pure Kitaev model with $\Gamma = \Gamma' = 0$. Figure 10(a) shows the temperature dependence of the specific heat of the classical Kitaev model at several magnetic fields along the [111] direction. In the absence of the magnetic field, previous studies have shown that the specific heat monotonically increases with decreasing temperature and approaches 3/4 in the zero temperature limit [73, 74]. This value originates from the zero modes that are intrinsic to the pure Kitaev model without a magnetic field, and the quartic order of the spin fluctuations contributes to the specific heat at $T \to 0$. Once the magnetic field is introduced, it lifts the zero modes, and thereby, the zero-T limit of the specific heat takes the conventional value, i.e., 1, owing to the presence of the two continuous variables (θ, ϕ) at each site. We find that it shows a shoulder-like structure at the temperature corresponding to the energy scale of h in the presence of the magnetic field despite the monotonic change at $h = 0$. In this temperature scale, the magnetization monotonically increases as a function of the magnetic field, as shown in Fig. 10(b).

Figure 10(c) shows the thermal Hall conductivity κ_{xy} as a function of temperature. When the magnetic field is not applied, κ_{xy} is always zero. By introducing the magnetic field, κ_{xy} becomes nonzero and positive, which is consistent with the results for the quantum system. Moreover, the temperature scale at which the thermal Hall conductivity develops is much smaller than that for the magnetization. The distinctly different temperature scales are similar to those in the quantum system [see Fig. 3] although the double-peak structure of the specific heat is not observed in the classical system. In the classical result, κ_{xy} shows a monotonic increase with decreasing temperature. On the other hand, in the quantum system, κ^{xy}/T exhibits a peak around the temperature at which the specific heat exhibits the low-T peak, as shown in Fig. 3(d). The difference is considered to originate from an artifact in the classical system, where the macroscopic degeneracy is present in the low-energy region. The degeneracy also causes the nonzero specific heat at zero temperature. Thus, the quantization of κ^{xy}/T does not occur in the classical system. Figures 10(d) and 10(e) present the three-body and two-body contributions of the thermal current to the thermal Hall conductivity, respectively. The two-body contribution $\kappa_{xy}^{(M)}$ is much smaller than the three-body one $\kappa_{xy}^{(L)}$, indicating that the thermal Hall effect is dominated by the three-body terms of the thermal current at the edges. This result is consistent with the quantum system, but the classical approximation appears not to reproduce small negative values of $\kappa_{xy}^{(M)}$ in weak magnetic fields as shown in Fig. 3(f). The difference suggests that the negative $\kappa_{xy}^{(M)}$ may be induced by quantum effects.

Next, we discuss the field-angle dependence of physical quantities in the pure Kitaev model. We consider three field directions $[11\bar{2}]$, $[\bar{1}10]$, and [111], which are perpendicular to each other. Figures 11(a) and 11(b) show the temperature dependence of the specific heat and magnetization along the corresponding field directions. These results indicate that the field direction hardly changes the specific heat and magnetization, which is also observed in the quantum system (see Fig. 5).

In contrast to these bulk physical quantities, the thermal Hall conductivity strongly depends on the direction of the applied magnetic field. As shown in Fig. 11(c), κ_{xy} is negative and decreases with decreasing temperature for $\boldsymbol{h} \parallel [11\bar{2}]$, whereas it is positive for $\boldsymbol{h} \parallel [111]$. Moreover, the absolute value for the former is smaller than that for the latter. While the overall behavior is consistent with that of the quantum system, the peak structure in Fig. 5(d) is not seen in the classical case. Furthermore, a large enhancement of $\kappa_{xy}^{(M)}$ at low temperatures for $\boldsymbol{h} \parallel [11\bar{2}]$ presented in Fig. 5(f) is not reproduced in the classical system as shown in Fig. 11(e) despite the similar temperature dependence of $\kappa_{xy}^{(L)}$ in the quantum and classical systems [Figs. 5(e) and 11(d)]. This result suggests that the three-body term can be understood in the classical picture, but quantum fluctuations beyond the classical approach substantially contribute to the two-body term. We also find that the thermal Hall conductivity is zero in the magnetic field applied along the $[\bar{1}10]$ direction, which is a consequence of the symmetry of the Hamiltonian, as discussed before.

Here, we introduce the Γ' and Γ interactions in the Kitaev model. First, we examine the effects of the Γ' interaction on the Kitaev system. Figure 12 shows the temperature dependence of physical quantities for several values of Γ' without the Γ interaction. A positive Γ' suppresses the specific heat and magnetization, whereas a negative Γ' enhances them. Moreover, we observe a peak in the specific heat at $\Gamma' = -0.02$ in Fig. 12, indicating its shift to higher temperatures with decreasing Γ'. These tendencies are also seen in the quantum system, as shown in Figs. 6(a) and 6(b).

Regarding thermal transport, we find that the negative (positive) Γ' enhances (suppresses) the thermal Hall conductivity [Fig. 12(c)]. We note that κ_{xy} becomes negative at low temperatures for $\Gamma' = 0.02$. We also find that the three-body part is the dominant contribution to the thermal Hall conductivity, as shown in Figs. 12(d) and 12(e). Thus, the overall tendency is consistent with that of the quantum systems. Furthermore, by examining the temperature dependence in detail, we find that results for the classical limit are in good agreement with those for the intermediate temperature range ($T \sim 0.05$) in the quantum system, as shown in Fig. 6(d). In the quantum systems around $T = 0.05$, κ_{xy} decrease monotonically by increasing Γ' and appears to be negative for $\Gamma' = 0.02$. Moreover, in this temperature range, $\kappa_{xy}^{(M)}$ is

much smaller than $\kappa_{xy}^{(L)}$, as shown in Figs. 6(e) and 6(f). These results indicate that κ_{xy} in the classical systems corresponds to κ_{xy} in the quantum systems at intermediate temperatures, where quantum fluctuations are expected to be small.

Finally, we examine the effect of the Γ term. Figure 13 shows the temperature dependence of physical quantities for several values of Γ, setting $\Gamma' = 0$. For negative Γ, the low-T specific heat is enhanced with increasing the absolute value of Γ, as shown in Fig. 13(a). On the other hand, the specific heat is suppressed by introducing a positive Γ. These tendencies are consistent with the results in the quantum system, whereas the peak structure shown in Fig. 8(a) is not reproduced in the classical simulations. Figure 13(b) shows the temperature dependence of the magnetization for several values of Γ. The magnetization increases with decreasing Γ, which is also observed in the quantum system, shown in Fig. 8(b).

Meanwhile, by comparing the effects of Γ' and Γ terms, we also find a behavior that is inconsistent with that in the quantum system. In the classical simulations, the specific heat and magnetization appear to be sensitive to Γ' rather than Γ, which is opposite to the results in the quantum system, as shown in Figs. 6 and 8. This contrasting behavior suggests that the Γ' interaction stabilizes spin states with weak quantum fluctuations, but quantum effects play important roles in the Kitaev-Γ model. Indeed, it has been pointed out that the Γ interaction does not destroy a QSL state [41, 75], whereas the introduction of Γ' shrinks the region of the QSL phase [50, 52].

While the Γ dependence of the specific heat and the magnetization is consistent with that in the quantum system, the low-temperature behavior of the thermal Hall conductivity [Fig. 13(c)] is significantly different from that of the quantum system shown in Fig. 8(d). A key feature of the quantum system is the substantial enhancement of both $\kappa_{xy}^{(L)}$ and $\kappa_{xy}^{(M)}$, which are almost canceled out in the total thermal Hall conductivity κ_{xy}. This is not reproduced in the classical system, suggesting that it originates from quantum fluctuations. Nevertheless, in the intermediate temperature region around $T = 0.05$ in Figs. 8(d)–8(f), we again find that the Γ and temperature dependencies are similar to the low-temperature behavior in the classical system, as shown in Figs. 13(c)–13(e). These results imply that the behavior in the intermediate temperature region of the quantum system can be understood within the classical regime because the effects of the quantum fluctuations are relatively weak.

D. Summary of temperature field dependence

In this section, we summarize the temperature and magnetic field dependence of κ_{xy} in both quantum and classical systems. In Figs. 14, we show the two-dimensional color plots of κ_{xy}/T as functions of temperature and magnetic field for various values of Γ and Γ', respectively. First, we observe that peaks in κ_{xy}/T appear in the h-T plane. We note that the peaks overshoot the half-quantized value. By introducing a weak Γ' interaction to the pure Kitaev model, a strong enhancements of κ_{xy}/T is observed for negative Γ', while positive Γ' suppresses κ_{xy}/T. The negative κ_{xy}/T observed for smaller h and lower temperature is probably due to the small D effects. In the case of Γ, we observe that negative Γ suppresses κ_{xy}/T, whereas positive Γ significantly enhances it at high magnetic fields. In addition, positive Γ makes κ_{xy}/T negative at small magnetic fields. By comparing $\Gamma = 0.01$ and 0.02, we observe that the region of negative κ_{xy}/T moves to higher magnetic fields. This trend might be related to a possible quantum phase transition, as discussed above.

In Fig. 15, we show the color plot of κ_{xy} in the h-T plane of the classical model. We can see that Γ term do not affects the overall behavior of κ_{xy}, while negative (positive) Γ' enhance (diminish) κ_{xy}. The insensitivity to the Γ term is in contrast to the results for quantum systems. Thus, the effects of Γ term are governed by the quantum effects while those of Γ' can be captured by the classical model.

V. SUMMARY AND DISCUSSION

In this study, we have conducted a systematic analysis of thermal Hall conductivity in the extended Kitaev model at finite temperatures using the tensor-network representation of the density matrix. This method enables a highly-accurate analysis of the thermal Hall conductivity beyond conventional perturbation theory. A key finding of this study is that the thermal Hall conductivity significantly exceeds the half-quantized value. This result indicates that the large thermal Hall conductivity observed in α-$RuCl_3$ experiments can be understood within the framework of the Kitaev model. We have demonstrated that the field-angle dependence of the thermal Hall conductivity remains consistent with the sign of the Chern number of Majorana fermions even in the high-magnetic-field regime. For the thermal Hall conductivity induced by the topological magnon, its sign is opposite to that observed in the present study [69]. In addition to the sign, its magnitude is smaller than the half-quantized value, indicating that the topological magnon alone may not be able to explain the overshooting of the thermal Hall conductivity.

Note that the overshoot of the thermal Hall conductivity beyond the half-quantized value has not been observed in the previous numerical study [33]. As we already mentioned, we have employed a proper position dependent representation for the poralization and have obtained the energy current as a vector, whereas the authors of [33] used a simplified treatment neglecting the directional dependence of energy currents. This treatment probably contributes to the significant difference in the calculated thermal Hall conductivities.

We have also demonstrated that the thermal Hall conductivity is significantly affected by the Γ and Γ' terms even when their magnitudes are two orders smaller than the Kitaev interaction. In particular, for negative Γ' and the positive Γ, the thermal Hall conductivity is enhanced. However, the mechanisms behind this enhancement are quite different. For negative Γ', we find that the enhancement is primarily driven by the three-body term $\kappa_{xy}^{(L)}$, which is consistent with the scenario where the negative Γ' term increases the Majorana gap [72]. In contrast, for positive Γ, the enhancement is governed by the two-body part $\kappa_{xy}^{(M)}$. This mechanism cannot be straightforwardly explained by perturbation theory and may be related to the possible phase transitions induced by the Γ term. By comparing the results in the quantum and classical systems, we find that the main effect of the Γ' term is well captured by classical systems, whereas the effect of the Γ term is not. In other words, the behavior of the three-body part $\kappa_{xy}^{(L)}$ can be reproduced by the classical model, whereas $\kappa_{xy}^{(M)}$ cannot. This result suggests that the Γ term exhibits stronger quantum effects.

Another important issue is the comparison between our results and the thermal Hall conductivity induced by topological magnons [69–71]. Although we observed a finite thermal Hall conductivity even at higher temperatures, its sign is different from the calculations assuming topological magnons. The origin of this discrepancy is not fully clear at moment. One possible origin might be the validity of the magnon picture at higher temperatures, where the magnetization is small. Another possible explanation involves the treatment of the edges in previous calculations on topological magnons, which assumed the bulk-edge correspondence and did not explicitly include the effects of the open edges, such as the reconstructions of magnetization around the edges [76, 77]. In contrast, in our calculation, we explicitly consider open boundaries and the thermal Hall conductivity is calculated based on the energy current at the edges. If the sign difference indeed originates from the edge treatment, our results might be relevant to the experimental observations because there are explicit edges in the experiments.

Our findings demonstrate the importance of developing methods that do not rely on specific quasiparticle assumptions. Most previous theoretical studies on the thermal Hall conductivity have focused on analyzing the contributions from the specific quasiparticles, such as the Majorana fermions and the topological magenons. In contrast, the method developed in this study enables the calculation of the thermal Hall conductivity in quantum spin systems without assuming specific quasiparticles. This approach provides a theoretical foundation for understanding experimental results, where the contributions from multiple quasiparticles may coexist. Given that thermal Hall conductivity measurements have been performed on a wide range of strongly correlated materials, our method offers a fundamental theoretical framework for their interpretation and serves as a useful tool for identifying exotic quasiparticles from experimental observations. This work paves the way for a more comprehensive understanding of the thermal Hall effect in strongly correlated materials.

ACKNOWLEDGMENTS

We wish to thank Y. Kato, K. Fukui, and K. Ido for fruitful discussions. This work was supported by Grant-in-Aid for Scientific Research Nos. 19H05825, 19K03742, 20H00122, 22H01179, 23K22450, and 23H03818 from the Ministry of Education, Culture, Sports, Science and Technology, Japan. It is also supported by JST CREST Grant No. JPMJCR18T2, JST PRESTO Grant No. JPMJPR19L5, and JST COI-NEXT Program Grant Number JPMJPF2221. This work was also supported by the National Natural Science Foundation of China (Grant No. 12150610462). Numerical calculations were performed using the facilities of the Supercomputer Center, The Institute for Solid State Physics, The University of Tokyo.

Appendix A: Benchmark on tensor network method

In this Appendix, we present several benchmark results for the XTRG method. First, we show dependence of the several representative physical quantities on bond dimension D for the pure Kitaev model on the $(L, L') = (6, 6)$ cylinder in Fig. 16. We find that the dependence on D becomes larger for the specific heat and the thermal Hall conductivity at $h = 0.04$ when $T \lesssim 0.05$. However, for $D = 500$, clear peak structures appear in the specific heat and the thermal Hall conductivity and their values deviate from those at $D = 400$. Thus, we conclude that $D = 500$ is sufficiently large to analyze the thermal Hall conductivity for $(L, L') = (6, 6)$, $T \geq 0.01$, and $h \geq 0.04$.

Next, for a different system size $(L, L') = (8, 4)$, we examine the bond-dimension dependence of the physical quantities. As shown in Fig. 17, for D up to 400, we obtained almost converged data even for the specific heat and the thermal Hall conductivity at $h = 0.04$. Although the accuracy of the matrix product representation depends on the circumference, i.e., the system size, we can obtain nearly converged results for $D = 400$. These results demonstrate that the XTRG method with a sufficiently large bond dimension D is a powerful tool for investigating the finite-temperature properties of quantum spin systems.

Appendix B: Benchmark on thermal pure quantum state

In this Appendix, we examine the accuracy of the cTPQ method by comparing its results with those of full diagonalization for a small $(L, L') = (2, 4)$ cluster (the

total system size is $N_s = 16$). In the full exact diagonalization (ED) method, we diagonalize the Hamiltonian, whose dimension is $2^{16} = 65536$ using ScaLAPACK [78]. Using the obtained eigenvalues and eigenvectors, we calculate the temperature dependence of physical quantities.

At $h = 0.04$, the specific heat C exhibits a three-peak structure in this system size. This structure may be an artifact of the small system size since it disappears in larger system sizes. Even at $h = 0.08$, a hump in the specific heat remains around $T = 0.02$. As shown in Fig. 18(a), the cTPQ method reproduces the temperature dependence of the specific heat for $h = 0.04$ and $h = 0.08$, including its three-peak structure. Figure 18(b) shows the temperature dependence of the magnetization. The cTPQ method also reproduces the results of full exact diagonalization.

We show the temperature dependence of the thermal Hall conductivity κ in Fig. 18(c). The thermal Hall conductivity κ at $|h| = 0.04$ becomes negative for $T \leq 0.01$. This negative κ may also result form finite-size effects, possibly due to the short length of the edges. In fact, κ becomes positive for larger system sizes, as we demonstrated above. The cTPQ method accurately captures this unusual temperature dependence. At $h = 0.08$, κ shows a single peak, which is also accurately reproduced by the cTPQ method. This agreement with full diagonalization demonstrate the reliablity of the cTPQ method.

Appendix C: Comparison between tensor network method and thermal pure quantum state

In this Appendix, we examine the accuracy of the XTRG method by comparing the results of the cTPQ method with those of the XTRG for the $(L, L') = (6, 2)$ cluster ($N_s = 24$). Figure 19(a) shows the temperature dependence of the specific heat. We find that both methods reproduce the two-peak structure in the specific heat, which is a characteristic feature of the Kitaev model. Apart from a small discrepancy near the low-temperature peak at $h = 0.04$, both methods show good agreement across three orders of magnitude in temperature. This consistency demonstrates that the XTRG method, with a sufficiently large bond dimension, provides accurate results.

In Fig. 19(b), we show the temperature dependence of the magnetization. Across all the temperature regions, we find that both methods show good agreement within the error bars. Since the magnetization is given by the first derivative of the free energy, its fluctuations are expected to be small. This may explain why the error bars of the magnetization are smaller than those of the specific heat and the thermal Hall conductivity.

We show the temperature dependence of κ in Fig. 19(c) and find that $D = 500$ already provides sufficiently accurate results of the thermal Hall conductivity κ except for the small deviations in its peak values. These results indicate that the XTRG calculations presented in this paper accurately capture the essential features of the thermal Hall conductivity in extended Kitaev models.

[1] A. Kitaev, Anyons in an exactly solved model and beyond, Ann. Phys. (N. Y.). **321**, 2 (2006).

[2] Y. Kasahara, T. Ohnishi, Y. Mizukami, O. Tanaka, S. Ma, K. Sugii, N. Kurita, H. Tanaka, J. Nasu, Y. Motome, T. Shibauchi, and Y. Matsuda, Majorana quantization and half-integer thermal quantum Hall effect in a Kitaev spin liquid, Nature **559**, 227 (2018).

[3] J. A. Sears, M. Songvilay, K. W. Plumb, J. P. Clancy, Y. Qiu, Y. Zhao, D. Parshall, and Y.-J. Kim, Magnetic order in $\alpha-rucl_3$: A honeycomb-lattice quantum magnet with strong spin-orbit coupling, Phys. Rev. B **91**, 144420 (2015).

[4] R. D. Johnson, S. C. Williams, A. A. Haghighirad, J. Singleton, V. Zapf, P. Manuel, I. I. Mazin, Y. Li, H. O. Jeschke, R. Valentí, and R. Coldea, Monoclinic crystal structure of $\alpha - rucl_3$ and the zigzag antiferromagnetic ground state, Phys. Rev. B **92**, 235119 (2015).

[5] H. B. Cao, A. Banerjee, J.-Q. Yan, C. A. Bridges, M. D. Lumsden, D. G. Mandrus, D. A. Tennant, B. C. Chakoumakos, and S. E. Nagler, Low-temperature crystal and magnetic structure of $\alpha-rucl_3$, Phys. Rev. B **93**, 134423 (2016).

[6] A. Banerjee, P. Lampen-Kelley, J. Knolle, C. Balz, A. A. Aczel, B. Winn, Y. Liu, D. Pajerowski, J. Yan, C. A. Bridges, *et al.*, Excitations in the field-induced quantum spin liquid state of α-rucl3, npj Quantum Materials **3**, 8 (2018).

[7] M. Yamashita, J. Gouchi, Y. Uwatoko, N. Kurita, and H. Tanaka, Sample dependence of half-integer quantized thermal Hall effect in the Kitaev spin-liquid candidate α-$RuCl_3$, Phys. Rev. B **102**, 220404 (2020).

[8] J. Bruin, R. Claus, Y. Matsumoto, N. Kurita, H. Tanaka, and H. Takagi, Robustness of the thermal hall effect close to half-quantization in α-rucl3, Nature Physics **18**, 401 (2022).

[9] T. Yokoi, S. Ma, Y. Kasahara, S. Kasahara, T. Shibauchi, N. Kurita, H. Tanaka, J. Nasu, Y. Motome, C. Hickey, S. Trebst, and Y. Matsuda, Half-integer quantized anomalous thermal Hall effect in the Kitaev material candidate α-$RuCl_3$, Science **373**, 568 (2021).

[10] M. Ye, G. B. Halász, L. Savary, and L. Balents, Quantization of the thermal hall conductivity at small hall angles, Phys. Rev. Lett. **121**, 147201 (2018).

[11] Y. Vinkler-Aviv and A. Rosch, Approximately quantized thermal hall effect of chiral liquids coupled to phonons, Phys. Rev. X **8**, 031032 (2018).

[12] A. P. Joy and A. Rosch, Dynamics of visons and thermal hall effect in perturbed kitaev models, Phys. Rev. X **12**, 041004 (2022).

[13] J. Chaloupka, G. Jackeli, and G. Khaliullin, Kitaev-

Heisenberg Model on a Honeycomb Lattice: Possible Exotic Phases in Iridium Oxides A_2IrO_3, Phys. Rev. Lett. **105**, 027204 (2010).
[14] J. Chaloupka, G. Jackeli, and G. Khaliullin, Zigzag Magnetic Order in the Iridium Oxide Na_2IrO_3, Phys. Rev. Lett. **110**, 097204 (2013).
[15] J. G. Rau, E. K.-H. Lee, and H.-Y. Kee, Generic spin model for the honeycomb iridates beyond the kitaev limit, Phys. Rev. Lett. **112**, 077204 (2014).
[16] J. G. Rau and H.-Y. Kee, Trigonal distortion in the honeycomb iridates: Proximity of zigzag and spiral phases in Na2IrO3 (2014).
[17] S. M. Winter, Y. Li, H. O. Jeschke, and R. Valentí, Challenges in design of kitaev materials: Magnetic interactions from competing energy scales, Phys. Rev. B **93**, 214431 (2016).
[18] P. Czajka, T. Gao, M. Hirschberger, P. Lampen-Kelley, A. Banerjee, J. Yan, D. G. Mandrus, S. E. Nagler, and N. Ong, Oscillations of the thermal conductivity in the spin-liquid state of α-rucl3, Nature Physics **17**, 915 (2021).
[19] P. Czajka, T. Gao, M. Hirschberger, P. Lampen-Kelley, A. Banerjee, N. Quirk, D. G. Mandrus, S. E. Nagler, and N. P. Ong, Planar thermal hall effect of topological bosons in the kitaev magnet α-rucl3, Nature Materials **22**, 36 (2023).
[20] P. A. McClarty, X.-Y. Dong, M. Gohlke, J. G. Rau, F. Pollmann, R. Moessner, and K. Penc, Topological magnons in kitaev magnets at high fields, Phys. Rev. B **98**, 060404 (2018).
[21] D. G. Joshi, Topological excitations in the ferromagnetic kitaev-heisenberg model, Phys. Rev. B **98**, 060405 (2018).
[22] R. Hentrich, M. Roslova, A. Isaeva, T. Doert, W. Brenig, B. Büchner, and C. Hess, Large thermal hall effect in $\alpha-rucl_3$: Evidence for heat transport by kitaev-heisenberg paramagnons, Phys. Rev. B **99**, 085136 (2019).
[23] E. Lefrançois, G. Grissonnanche, J. Baglo, P. Lampen-Kelley, J.-Q. Yan, C. Balz, D. Mandrus, S. E. Nagler, S. Kim, Y.-J. Kim, N. Doiron-Leyraud, and L. Taillefer, Evidence of a phonon hall effect in the kitaev spin liquid candidate $\alpha-rucl_3$, Phys. Rev. X **12**, 021025 (2022).
[24] J. Nasu, M. Udagawa, and Y. Motome, Vaporization of kitaev spin liquids, Phys. Rev. Lett. **113**, 197205 (2014).
[25] J. Nasu, M. Udagawa, and Y. Motome, Thermal fractionalization of quantum spins in a kitaev model: Temperature-linear specific heat and coherent transport of majorana fermions, Phys. Rev. B **92**, 115122 (2015).
[26] J. Yoshitake, J. Nasu, and Y. Motome, Fractional spin fluctuations as a precursor of quantum spin liquids: Majorana dynamical mean-field study for the kitaev model, Phys. Rev. Lett. **117**, 157203 (2016).
[27] J. Yoshitake, J. Nasu, Y. Kato, and Y. Motome, Majorana dynamical mean-field study of spin dynamics at finite temperatures in the honeycomb kitaev model, Phys. Rev. B **96**, 024438 (2017).
[28] J. Yoshitake, J. Nasu, and Y. Motome, Temperature evolution of spin dynamics in two- and three-dimensional kitaev models: Influence of fluctuating Z_2 flux, Phys. Rev. B **96**, 064433 (2017).
[29] J. Yoshitake, J. Nasu, Y. Kato, and Y. Motome, Majorana-magnon crossover by a magnetic field in the kitaev model: Continuous-time quantum monte carlo study, Phys. Rev. B **101**, 100408 (2020).
[30] J. Nasu, J. Yoshitake, and Y. Motome, Thermal transport in the kitaev model, Phys. Rev. Lett. **119**, 127204 (2017).
[31] D. Takikawa and S. Fujimoto, Topological phase transition to abelian anyon phases due to off-diagonal exchange interaction in the kitaev spin liquid state, Phys. Rev. B **102**, 174414 (2020).
[32] M. G. Yamada and S. Fujimoto, Quantum liquid crystals in the finite-field kγ model for $\alpha-rucl_3$ (2021).
[33] A. Kumar and V. Tripathi, Thermal hall conductivity near field-suppressed magnetic order in a kitaev-heisenberg model, Phys. Rev. B **107**, L220406 (2023).
[34] G. Jackeli and G. Khaliullin, Mott Insulators in the Strong Spin-Orbit Coupling Limit: From Heisenberg to a Quantum Compass and Kitaev Models, Phys. Rev. Lett. **102**, 017205 (2009).
[35] Y. Yamaji, Y. Nomura, M. Kurita, R. Arita, and M. Imada, First-principles study of the honeycomb-lattice iridates na_2iro_3 in the presence of strong spin-orbit interaction and electron correlations, Phys. Rev. Lett. **113**, 107201 (2014).
[36] S. M. Winter, A. A. Tsirlin, M. Daghofer, J. van den Brink, Y. Singh, P. Gegenwart, and R. Valentí, Models and materials for generalized kitaev magnetism, J. Phys.: Condens. Matter **29**, 493002 (2017).
[37] Y. Yamaji, T. Suzuki, T. Yamada, S.-i. Suga, N. Kawashima, and M. Imada, Clues and criteria for designing a kitaev spin liquid revealed by thermal and spin excitations of the honeycomb iridate na_2iro_3, Phys. Rev. B **93**, 174425 (2016).
[38] T. Suzuki and S.-i. Suga, Effective model with strong kitaev interactions for $\alpha-rucl_3$, Phys. Rev. B **97**, 134424 (2018).
[39] P. Laurell and S. Okamoto, Dynamical and thermal magnetic properties of the kitaev spin liquid candidate α-rucl 3, npj Quantum Materials **5**, 1 (2020).
[40] P. A. Maksimov and A. L. Chernyshev, Rethinking $\alpha-rucl_3$, Phys. Rev. Res. **2**, 033011 (2020).
[41] A. Catuneanu, Y. Yamaji, G. Wachtel, Y. B. Kim, and H.-Y. Kee, Path to stable quantum spin liquids in spin-orbit coupled correlated materials, npj Quantum Materials **3**, 23 (2018).
[42] T. Yamada, T. Suzuki, and S.-i. Suga, Ground-state properties of the $k-\Gamma$ model on a honeycomb lattice, Phys. Rev. B **102**, 024415 (2020).
[43] M. Gohlke, G. Wachtel, Y. Yamaji, F. Pollmann, and Y. B. Kim, Quantum spin liquid signatures in kitaev-like frustrated magnets, Phys. Rev. B **97**, 075126 (2018).
[44] H.-Y. Lee, R. Kaneko, L. E. Chern, T. Okubo, Y. Yamaji, N. Kawashima, and Y. B. Kim, Magnetic field induced quantum phases in a tensor network study of kitaev magnets, Nature communications **11**, 1639 (2020).
[45] X.-Y. Zhang, S. Liang, H.-J. Liao, W. Li, and L. Wang, Differentiable programming tensor networks for kitaev magnets, Phys. Rev. B **108**, 085103 (2023).
[46] S.-S. Zhang, G. B. Halász, W. Zhu, and C. D. Batista, Variational study of the kitaev-heisenberg-gamma model, Phys. Rev. B **104**, 014411 (2021).
[47] R. L. Smit, S. Keupert, O. Tsyplyatyev, P. A. Maksimov, A. L. Chernyshev, and P. Kopietz, Magnon damping in the zigzag phase of the kitaev-heisenberg-Γ model on a honeycomb lattice, Phys. Rev. B **101**, 054424 (2020).
[48] A. Rayyan, Q. Luo, and H.-Y. Kee, Extent of frustration

in the classical kitaev-Γ model via bond anisotropy, Phys. Rev. B **104**, 094431 (2021).
[49] Q. Luo, P. P. Stavropoulos, J. S. Gordon, and H.-Y. Kee, Spontaneous chiral-spin ordering in spin-orbit coupled honeycomb magnets, Phys. Rev. Res. **4**, 013062 (2022).
[50] Q. Luo and H.-Y. Kee, Interplay of magnetic field and trigonal distortion in the honeycomb Γ model: Occurrence of a spin-flop phase, Phys. Rev. B **105**, 174435 (2022).
[51] J. Rusnačko, D. Gotfryd, and J. c. v. Chaloupka, Kitaev-like honeycomb magnets: Global phase behavior and emergent effective models, Phys. Rev. B **99**, 064425 (2019).
[52] J. S. Gordon, A. Catuneanu, E. S. Sørensen, and H.-Y. Kee, Theory of the field-revealed kitaev spin liquid, Nature communications **10**, 1 (2019).
[53] L. E. Chern, R. Kaneko, H.-Y. Lee, and Y. B. Kim, Magnetic field induced competing phases in spin-orbital entangled kitaev magnets, Phys. Rev. Res. **2**, 013014 (2020).
[54] H. Katsura, N. Nagaosa, and P. A. Lee, Theory of the thermal hall effect in quantum magnets, Phys. Rev. Lett. **104**, 066403 (2010).
[55] B. B. Chen, L. Chen, Z. Chen, W. Li, and A. Weichselbaum, Exponential Thermal Tensor Network Approach for Quantum Lattice Models, Phys. Rev. X **8**, 31082 (2018).
[56] H. Li, D.-W. Qu, H.-K. Zhang, Y.-Z. Jia, S.-S. Gong, Y. Qi, and W. Li, Universal thermodynamics in the Kitaev fractional liquid, Phys. Rev. Res. **2**, 043015 (2020), 2006.02405.
[57] H. Li, H.-K. Zhang, J. Wang, H.-Q. Wu, Y. Gao, D.-W. Qu, Z.-X. Liu, S.-S. Gong, and W. Li, Identification of magnetic interactions and high-field quantum spin liquid in α -rucl3, Nature Communications **12**, 4007 (2021).
[58] S. Sugiura and A. Shimizu, Canonical thermal pure quantum state, Phys. Rev. Lett. **111**, 010401 (2013).
[59] M. Imada and M. Takahashi, Quantum transfer monte carlo method for finite temperature properties and quantum molecular dynamics method for dynamical correlation functions, J. Phys. Soc. Jpn. **55**, 3354 (1986).
[60] J. Jaklič and P. Prelovšek, Lanczos method for the calculation of finite-temperature quantities in correlated systems, Phys. Rev. B **49**, 5065 (1994).
[61] A. Hams and H. De Raedt, Fast algorithm for finding the eigenvalue distribution of very large matrices, Phys. Rev. E **62**, 4365 (2000).
[62] S. Lloyd, Pure state quantum statistical mechanics and black holes, arXiv:1307.0378 https://doi.org/10.48550/arXiv.1307.0378.
[63] M. Kawamura, K. Yoshimi, T. Misawa, Y. Yamaji, S. Todo, and N. Kawashima, Quantum lattice model solver HΦ, Computer Physics Communications **217**, 180 (2017).
[64] K. Ido, M. Kawamura, Y. Motoyama, K. Yoshimi, Y. Yamaji, S. Todo, N. Kawashima, and T. Misawa, Update of $\mathcal{H}\phi$: Newly added functions and methods in versions 2 and 3, Comp. Phys. Commun. **298**, 109093 (2024).
[65] https://github.com/issp-center-dev/HPhi/releases.
[66] K. Hukushima and K. Nemoto, Exchange Monte Carlo Method and Application to Spin Glass Simulations, J. Phys. Soc. Japan **65**, 1604 (1996).
[67] H. Li, E. Lv, N. Xi, Y. Gao, Y. Qi, W. Li, and G. Su, Magnetocaloric effect of topological excitations in kitaev magnets, Nature Communications **15**, 7011 (2024).
[68] H.-C. Jiang, Z.-C. Gu, X.-L. Qi, and S. Trebst, Possible proximity of the mott insulating iridate na_2iro_3 to a topological phase: Phase diagram of the heisenberg-kitaev model in a magnetic field, Phys. Rev. B **83**, 245104 (2011).
[69] P. A. McClarty, X.-Y. Dong, M. Gohlke, J. G. Rau, F. Pollmann, R. Moessner, and K. Penc, Topological magnons in kitaev magnets at high fields, Phys. Rev. B **98**, 060404 (2018).
[70] D. G. Joshi, Topological excitations in the ferromagnetic kitaev-heisenberg model, Phys. Rev. B **98**, 060405 (2018).
[71] L. E. Chern, E. Z. Zhang, and Y. B. Kim, Sign structure of thermal hall conductivity and topological magnons for in-plane field polarized kitaev magnets, Phys. Rev. Lett. **126**, 147201 (2021).
[72] D. Takikawa and S. Fujimoto, Topological phase transition to abelian anyon phases due to off-diagonal exchange interaction in the kitaev spin liquid state, Phys. Rev. B **102**, 174414 (2020).
[73] E. Sela, H.-C. Jiang, M. H. Gerlach, and S. Trebst, Order-by-disorder and spin-orbital liquids in a distorted heisenberg-kitaev model, Phys. Rev. B **90**, 035113 (2014).
[74] T. Suzuki and Y. Yamaji, Thermal properties of spin-s kitaev-heisenberg model on a honeycomb lattice, Physica B: Condensed Matter **536**, 637 (2018).
[75] M. Gohlke, G. Wachtel, Y. Yamaji, F. Pollmann, and Y. B. Kim, Quantum spin liquid signatures in kitaev-like frustrated magnets, Phys. Rev. B **97**, 075126 (2018).
[76] S. Koyama and J. Nasu, Flavor-wave theory with quasiparticle damping at finite temperatures: Application to chiral edge modes in the kitaev model, Phys. Rev. B **108**, 235162 (2023).
[77] J. Habel, A. Mook, J. Willsher, and J. Knolle, Breakdown of chiral edge modes in topological magnon insulators, Phys. Rev. B **109**, 024441 (2024).
[78] L. S. Blackford, J. Choi, A. Cleary, E. D'Azevedo, J. Demmel, I. Dhillon, J. Dongarra, S. Hammarling, G. Henry, A. Petitet, K. Stanley, D. Walker, and R. C. Whaley, *ScaLAPACK Users' Guide* (Society for Industrial and Applied Mathematics, Philadelphia, PA, 1997).

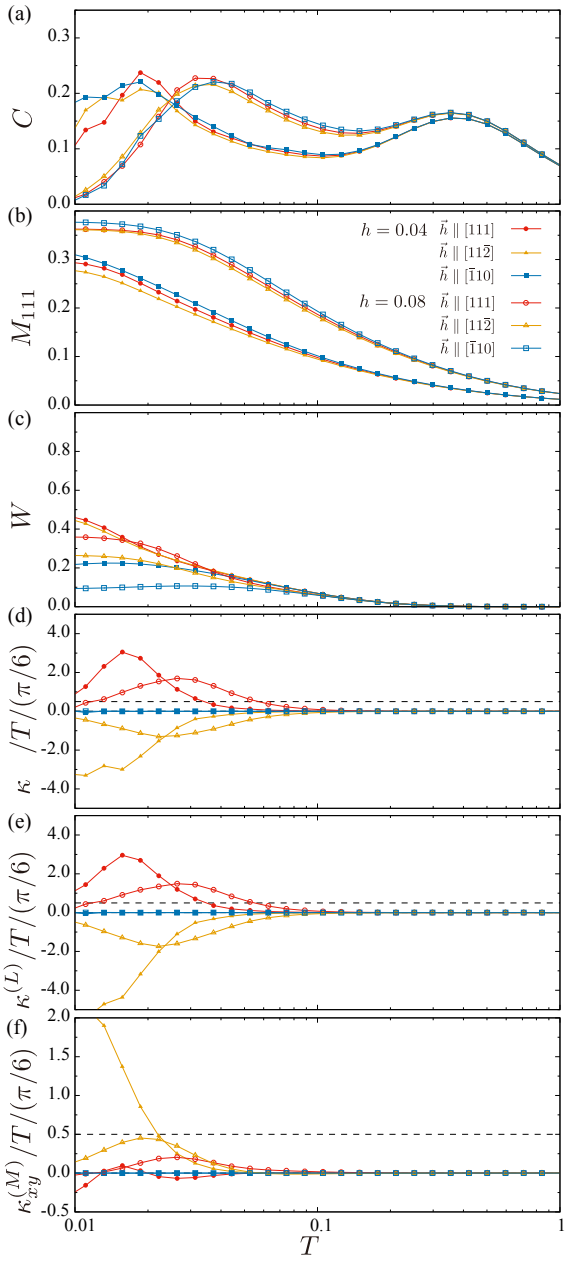

FIG. 5. Temperature dependence of (a) the specific heat, (b) the magnetic moment, (c) the flux, and (d) κ_{xy}/T of the ferromagnetic Kitaev model under magnetic fields parallel to [111], [11$\bar{2}$], and [1$\bar{1}$0] with $h = 0.04$ and $h = 0.08$. (e),(f) Contributions from the three-spin term in Eq. (7) and the two-spin term in Eq. (8) to κ_{xy}/T, respectively. The data in (d), (e), and (f) are plotted in units of $\pi/6$, and the horizontal dashed lines indicate the half-integer quantized value $\kappa_{xy}/T = \pi/12$.

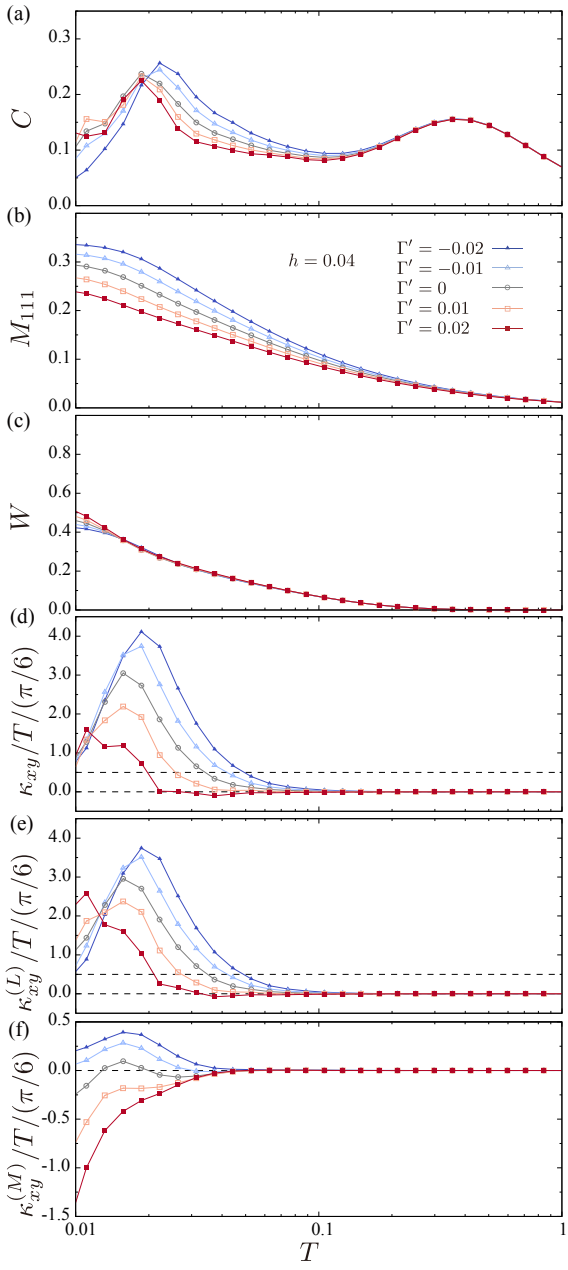

FIG. 6. Temperature dependence of (a) the specific heat (b) the magnetic moment, (c) the flux (d) the total thermal Hall conductivity κ_{xy}/T, (e) the three-body part of the thermal Hall conductivity $\kappa_{xy}^{(L)}/T$, and (f) the two-body part of the thermal Hall conductivity $\kappa_{xy}^{(M)}/T$ of the extended Kitaev model with $\Gamma = 0$ and varying Γ' under a magnetic field parallel to [111] direction. The amplitude of the magnetic field is $|h| = 0.04$.

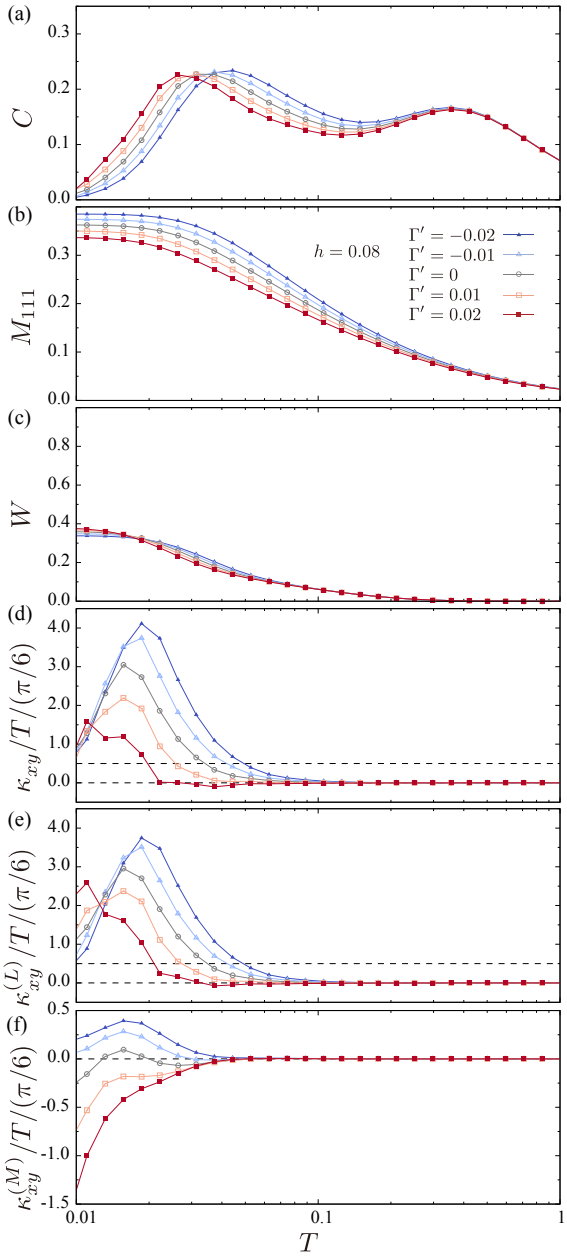

FIG. 7. Corresponding plots to Fig. 6 for the extended Kitaev model with $\Gamma = 0$, $h = 0.08$ and varying Γ'.

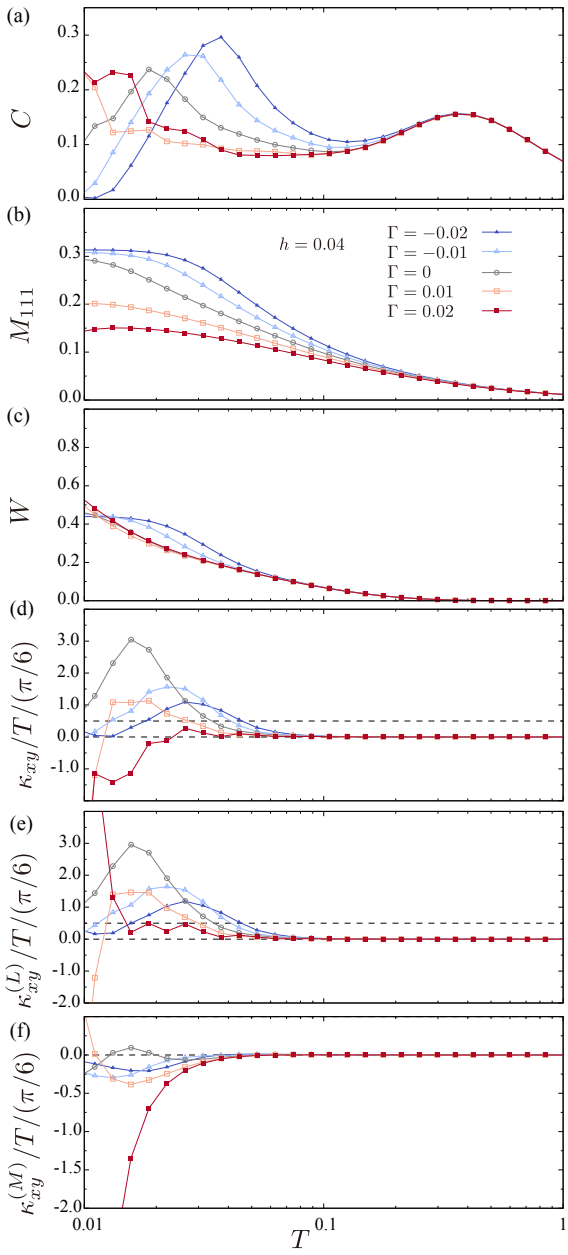

FIG. 8. Corresponding plots to Fig. 6 for the extended Kitaev model with $\Gamma' = 0$, $h = 0.04$ and varying Γ.

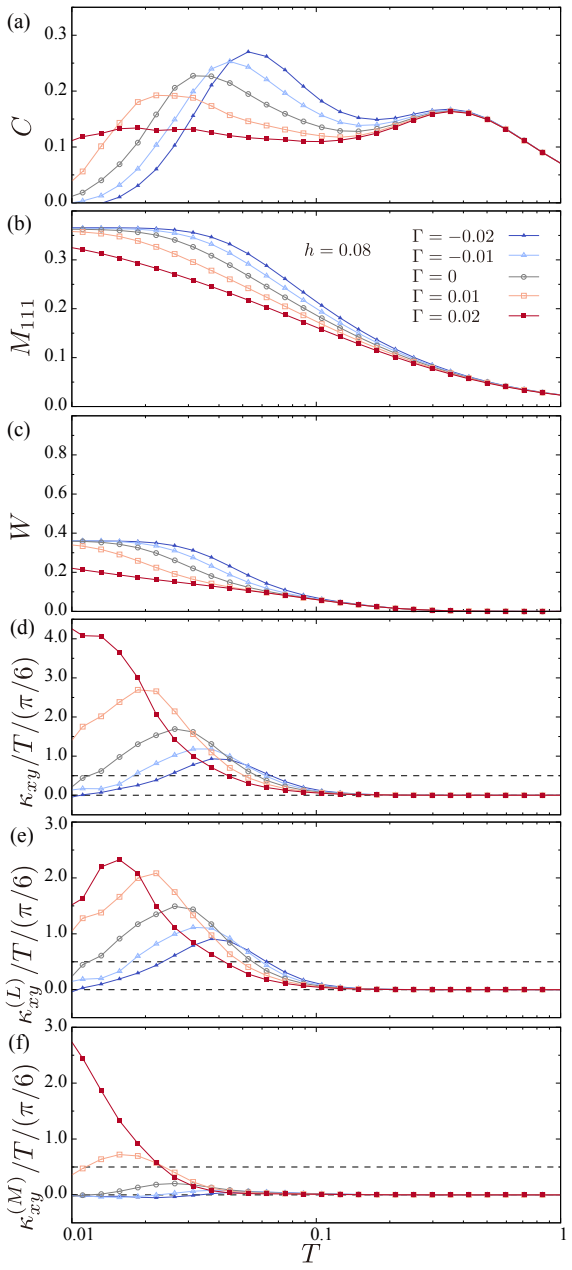

FIG. 9. Corresponding plots to Fig. 6 for the extended Kitaev model with $\Gamma' = 0$, $h = 0.08$ and varying Γ.

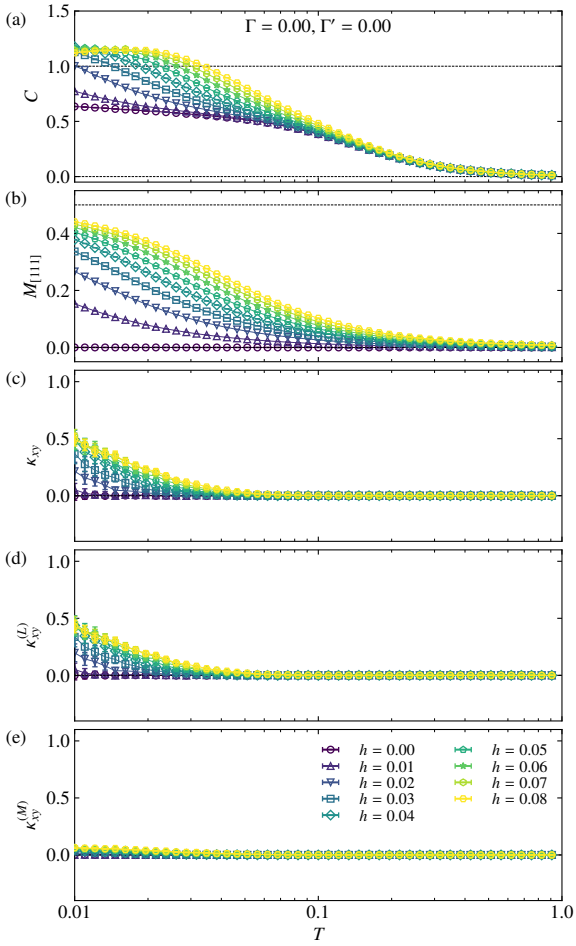

FIG. 10. Temperature dependence of (a) the specific heat, (b) the total magnetization, and (c) the thermal Hall conductivity κ_{xy} for several magnetic fields along the [111] direction in the classical Kitaev model. (d),(e) Temperature dependence of the two components, (L) and (M), of the thermal Hall conductivity.

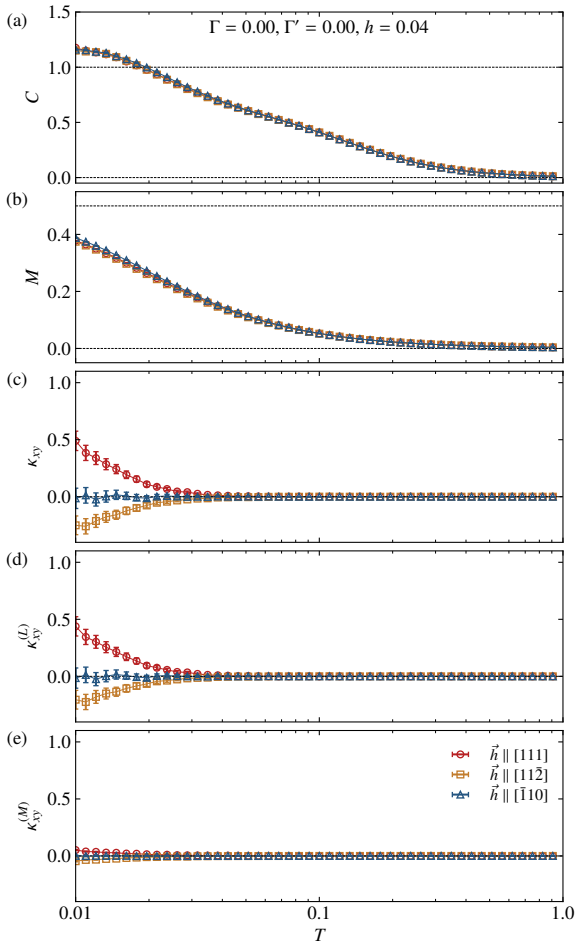

FIG. 11. Temperature dependence of (a) the specific heat, (b) the total magnetization, and (c) the thermal Hall conductivity κ_{xy} in the classical Kitaev model under the magnetic field parallel to [111], [11$\bar{2}$], and [$\bar{1}$10] with $h = 0.04$. (d),(e) Temperature dependence of the two components, (L) and (M), of the thermal Hall conductivity.

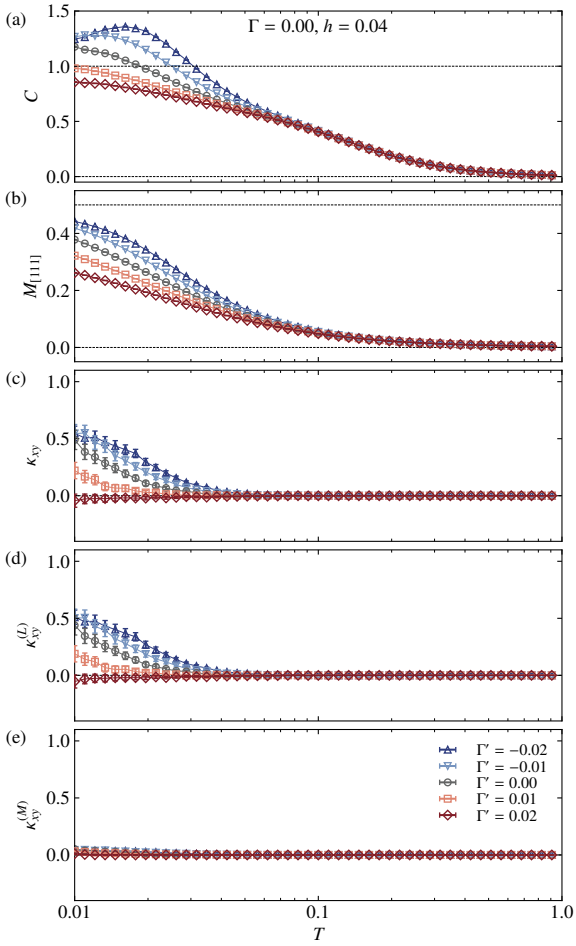

FIG. 12. Temperature dependence of (a) the specific heat, (b) the total magnetization, and (c) the thermal Hall conductivity κ_{xy} in the classical Kitaev-Γ' model under the magnetic field with $h = 0.04$. (d),(e) Temperature dependence of the two components, (L) and (M), of the thermal Hall conductivity.

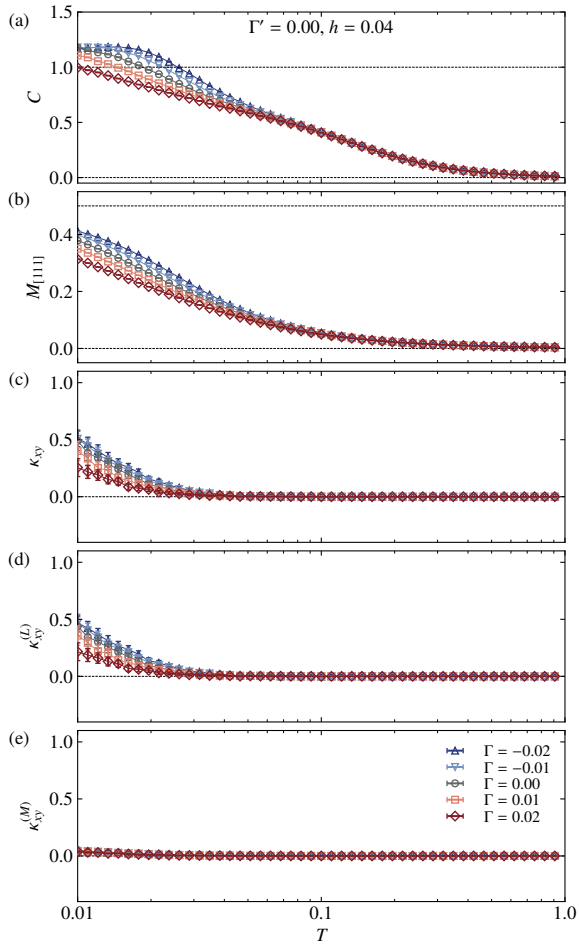

FIG. 13. Temperature dependence of (a) the specific heat, (b) the total magnetization, and (c) the thermal Hall conductivity κ_{xy} in the classical Kitaev-Γ model under the magnetic field with $h = 0.04$. (d),(e) Temperature dependence of the two components, (L) and (M), of the thermal Hall conductivity.

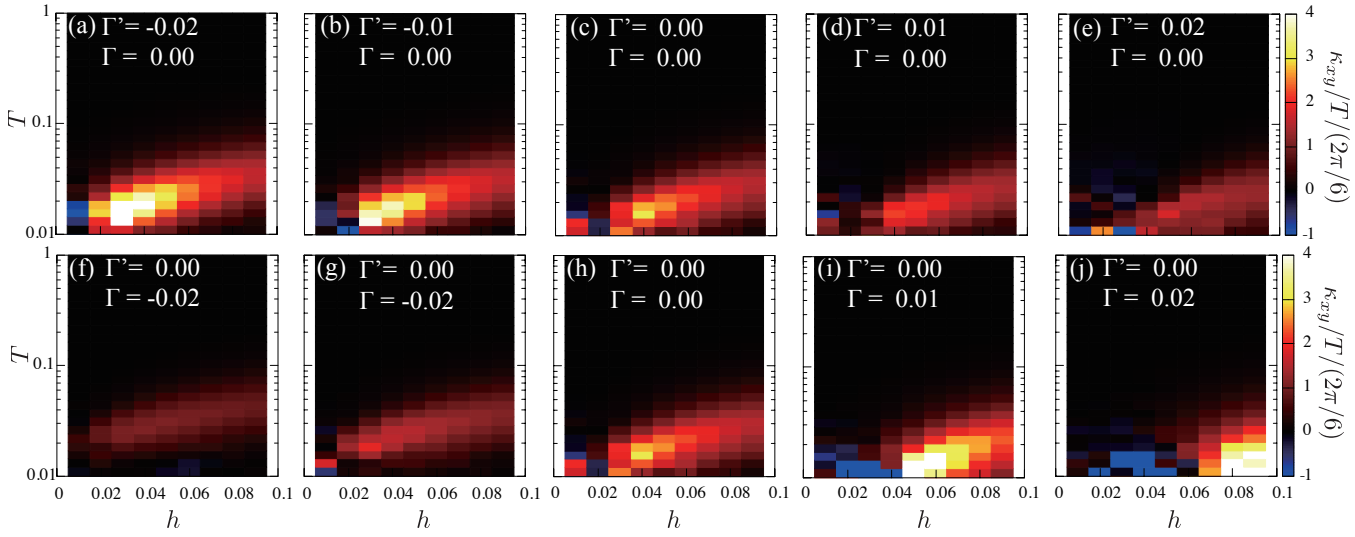

FIG. 14. (a)-(e) Color maps of κ_{xy}/T for ferromagnetic Kitaev model with $\Gamma = 0, \pm 0.01, \pm 0.02$ with various magnetic fields and temperatures. (f)-(j) Color maps of κ_{xy}/T for ferromagnetic Kitaev model with $\Gamma' = 0, \pm 0.01, \pm 0.02$ with various magnetic fields and temperatures.

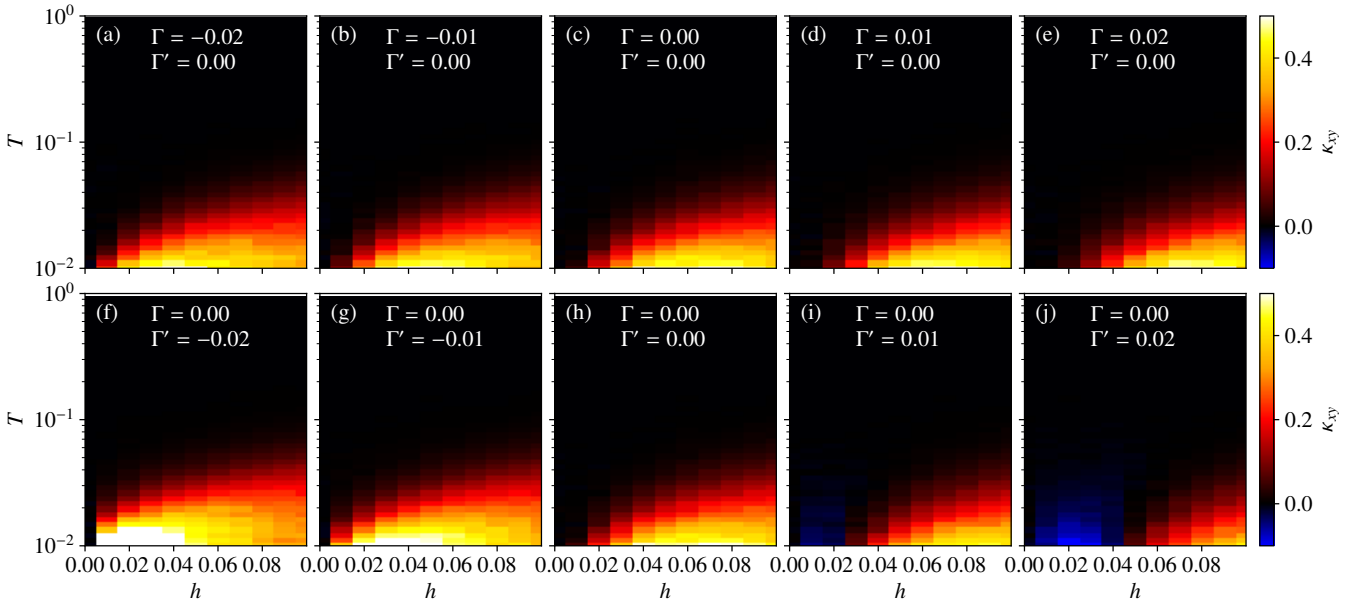

FIG. 15. Corresponding plots to Fig. 14 for the classical model.

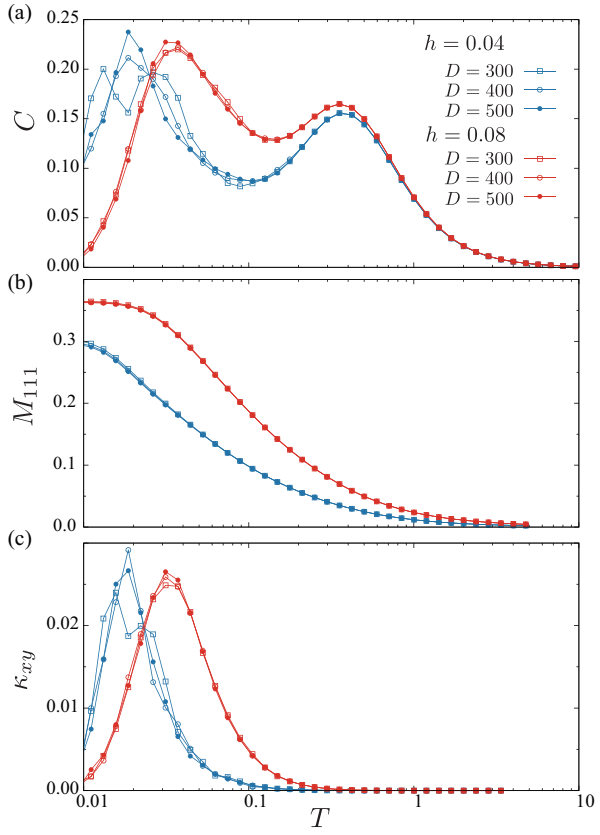

FIG. 16. Temperature dependence of (a) the specific heat (b) the magnetic moment, and (c) the thermal Hall conductivity of the ferromagnetic Kitaev model for the external magnetic field $h = 0.04$ and $h = 0.08$ parallel to [111] direction with different bond-dimensions $D = 300, 400, 500$. The lattice is $(L, L') = (6, 6)$

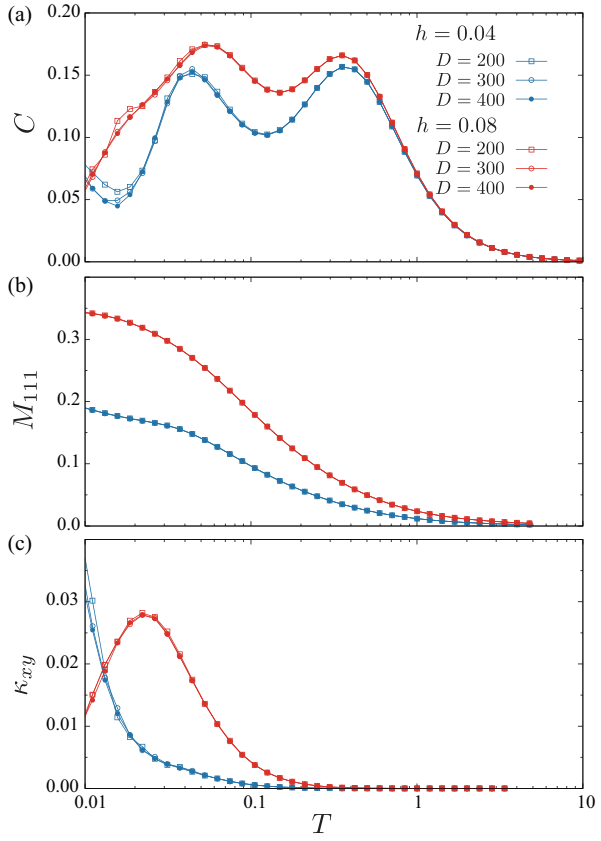

FIG. 17. Corresponding plot to Fig. 16 for $(L, L') = (8, 4)$.

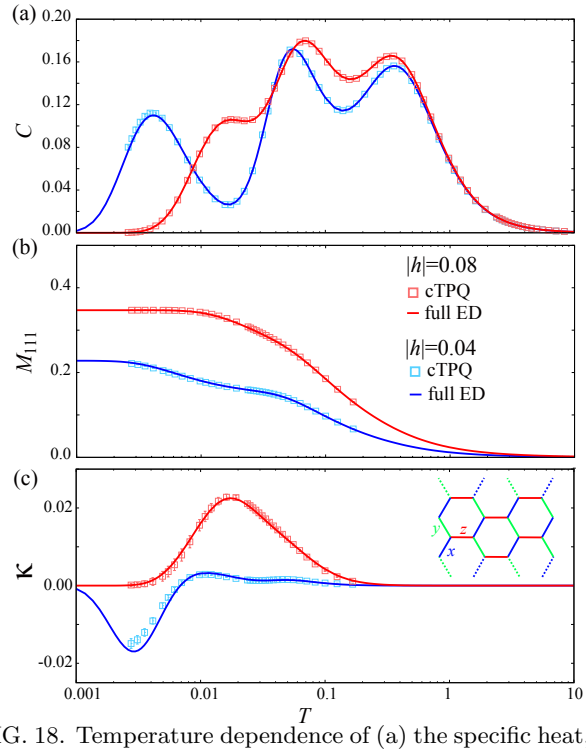

FIG. 18. Temperature dependence of (a) the specific heat, (b) the total magnetization, and (c) the thermal Hall conductivity κ. In the bootstrap sampling, we take 1000 independent initial states and choose 1000 samples 500 times with replacement to evaluate the average values and the error vars.

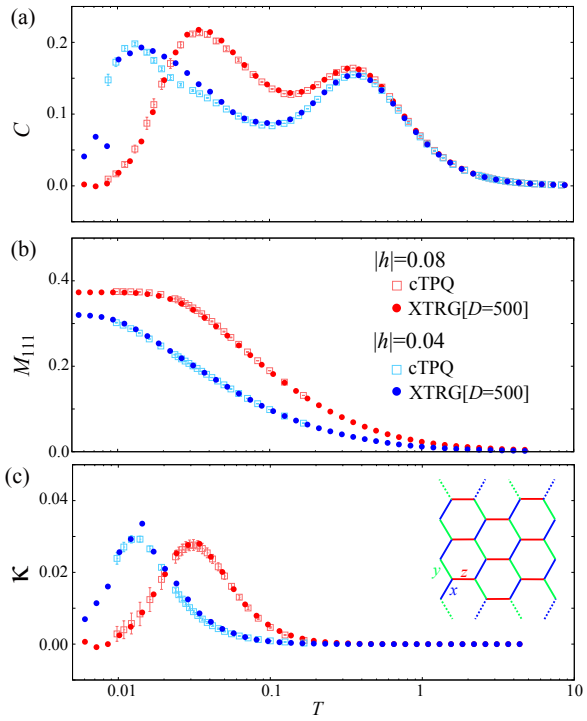

FIG. 19. Temperature dependence of (a) the specific heat, (b) the total magnetization, and (c) the thermal Hall conductivity κ. In the bootstrap sampling, we take 100 independent initial states, and choose 100 samples 50 times with replacement to evaluate the average values and the error vars.